

# The water vapor budget of a hurricane as dependent on its movement

Anastassia M. Makarieva<sup>1,2\*</sup>, Victor G. Gorshkov<sup>1,2</sup>,  
Andrei V. Nefiodov<sup>1</sup>, Alexander V. Chikunov<sup>3,4</sup>, Douglas Sheil<sup>5</sup>,  
Antonio Donato Nobre<sup>6</sup>, and Bai-Lian Li<sup>2</sup>

<sup>1</sup>Theoretical Physics Division, Petersburg Nuclear Physics Institute, 188300 Gatchina, St. Petersburg, Russia. <sup>2</sup>USDA-China MOST Joint Research Center for AgroEcology and Sustainability, University of California, Riverside 92521-0124, USA. <sup>3</sup>Institute of World Ideas, Udaltsova street 1A, 119415 Moscow, Russia. <sup>4</sup>Princeton Institute of Life Sciences, Princeton, USA. <sup>5</sup>Norwegian University of Life Sciences, Ås, Norway. <sup>6</sup>Centro de Ciência do Sistema Terrestre INPE, São José dos Campos SP 12227-010, Brazil.

## Abstract

Despite the dangers associated with tropical cyclones and their rainfall, the origins of storm moisture remains unclear. Existing studies have focused on the region 40-400 km from the cyclone center. It is known that the rainfall within this area cannot be explained by local processes alone but requires imported moisture. Nonetheless, the dynamics of this imported moisture appears unknown. Here, considering a region up to three thousand kilometers from storm center, we analyze precipitation, atmospheric moisture and movement velocities for North Atlantic hurricanes. Our findings indicate that even over such large areas a hurricane's rainfall cannot be accounted for by concurrent evaporation. We propose instead that a hurricane consumes pre-existing atmospheric water vapor as it moves. The propagation velocity of the cyclone, i.e. the difference between its movement velocity and the mean velocity of the surrounding air (steering flow), determines the water vapor budget. Water vapor available to the hurricane through its movement makes the hurricane self-sufficient at about 700 km from the hurricane center obviating the need to concentrate moisture from greater distances. Such hurricanes leave a dry wake, whereby rainfall is suppressed by up to 40% compared to its long-term mean. The inner radius of this dry footprint approximately coincides with the radius of hurricane self-sufficiency with respect to water vapor. We discuss how Carnot efficiency considerations do not constrain the power of such open systems that deplete the pre-existing moisture. Our findings emphasize the incompletely understood role and importance of atmospheric moisture supplies, condensation and precipitation in hurricane dynamics.

---

\* *Corresponding author.* E-mail: ammakarieva@gmail.com

# 1 Introduction

Intense tropical cyclones, also called hurricanes and typhoons depending on their locations, are associated with intense rainfall (Rodgers et al., 1994; Lonfat et al., 2004). For example, the mean rainfall within an Atlantic hurricane of 400 km radius is about 2 mm h<sup>-1</sup>. Such rainfall is ten times the long-term mean of tropical oceanic evaporation and could deplete local atmospheric moisture within a day. However, hurricanes can sustain this rainfall for several days, during which their atmospheric moisture content remains constant or even grows. How do hurricanes achieve that?

Most empirical and modelling studies investigating the water budget of tropical cyclones have focused on the inner area within 400 km from the cyclone center. For Atlantic hurricanes  $r_o = 400$  km corresponds to the mean radius of the outermost closed isobar. Within this area the local source of moisture (evaporation from the ocean) was estimated to be about 10-20% of total rainfall (Table 1). This means that most moisture is imported from the outer region (Fig. 1).

Using the assumption that the cyclone is sustained by concurrent evaporation, many theoretical studies have viewed tropical cyclones as steady-state thermodynamic systems which persist as long as they can consume moisture from the ocean (Emanuel, 1986; Pauluis, 2011; Sabuwala et al., 2015; Ozawa and Shimokawa, 2015; Kieu, 2015). But, while oceanic evaporation within the cyclone area  $r \leq r_o$  increases with wind speed and thus exceeds its long-term mean value, the available estimates show that this is insufficient to sustain rainfall (Table 1).

On the other hand, long-term mean oceanic evaporation concurrent with the cyclone *could* provide sufficient water vapor to sustain a high rainfall hurricane if this vapor were imported from a large area of 1500-2000 km around the hurricane center (Anthes, 1974; Trenberth et al., 2003). This radius is 3-5 times larger than that of the hurricane rainfall area. To concentrate this moisture requires a radial pressure gradient to drive moist air towards the storm's center. However, the radial pressure gradient in tropical cyclones is known to decline to near-zero values at distances of a few hundred kilometers from the storm's center (e.g., Holland, 2008). There are neither empirical nor theoretical evaluations of the ability of such pressure gradients to drive sufficient moisture convergence across several thousand kilometers. Thus, despite the dangers associated with tropical cyclone rainfall and the need for improved predictions (Rappaport, 2000), there is no clarity as to how this rainfall is generated and maintained.

Here we consider moisture dynamics in North Atlantic hurricanes up to 3000 km from the hurricane center. We first present theoretical considerations which explain observed evaporation-to-rainfall ratios (Section 2). These considerations demonstrate that observations do not support the notion that hurricane-related rainfall is provided by evaporation concurrent with the hurricane, however large the spatial scale. We then use data from the Tropical Rainfall Measuring Mission (TRMM) (Huffman et al., 2007) and Modern Era Retrospective Re-Analysis for Research and Applications (MERRA) (Rienecker et al.,

2011) to study rainfall and atmospheric moisture content in the vicinity of selected hurricanes (Sections 3 and 4).

Based on this analysis, we formulate a novel view of hurricane water budgets (Section 5). We show that the water vapor expenditures of a hurricane can be explained by considering its large-scale motion: the hurricane depletes pre-existing atmospheric water vapor as it moves through the atmosphere. In this manner the hurricane becomes self-sustaining for water vapor over a region of just about 700 km from its center. In the frame of reference co-moving with the storm there is a flow of moist ambient air towards the hurricane. This flow, which is proportional to the velocity of hurricane’s movement, delivers water vapor to the hurricane obviating the need to concentrate moisture from far outside.

We discuss the implications of our findings for understanding hurricanes, their rainfall and their power. We emphasize that the processes by which hurricanes and other cyclonic storms obtain their moisture, either by concurrent evaporation or by depletion of pre-existing stores of water vapor, are key for finding constraints on their intensity (Section 6). In the concluding section we discuss perspectives for further research.

## 2 Water vapor budget of a tropical cyclone

We start by expressing evaporation-to-precipitation ratios via measurable atmospheric parameters. Consider an air parcel containing  $\tilde{N}$  moles of air,  $\tilde{N}_d$  moles of dry air and  $\tilde{N}_v$  moles of water vapor,  $\tilde{N} = \tilde{N}_d + \tilde{N}_v$ . It begins spiralling in the boundary layer from outside the hurricane towards the area of maximum winds (the windwall), see points A and B in Fig. 1. If our air parcel gathers water vapor evaporating from the oceanic surface beneath the parcel’s trajectory, the ratio  $\gamma_d \equiv \tilde{N}_v/\tilde{N}_d = N_v/N_d$  must grow. Here  $N_v \equiv \tilde{N}_v/\tilde{V}$  and  $N_d \equiv \tilde{N}_d/\tilde{V}$  (mol m<sup>-3</sup>) are molar densities of water vapor and dry air, respectively;  $\tilde{V}$  is the parcel’s volume.

Using the ideal gas law

$$p = NRT, \tag{1}$$

where  $p = p_v + p_d$  is air pressure,  $p_v$  and  $p_d$  are partial pressures of water vapor and dry air,  $T$  is temperature,  $N = N_v + N_d$  is air molar density and  $R = 8.3 \text{ J mol}^{-1} \text{ K}^{-1}$  is the universal gas constant, the definitions of  $\gamma_d \equiv N_v/N_d = p_v/p_d$ ,  $\gamma \equiv p_v/p$  and relative humidity  $H \equiv p_v/p_v^*$ , where  $p_v^*$  is saturated pressure of water vapor, we have:

$$\frac{d\gamma_d}{\gamma_d} = \frac{1}{1 - \gamma} \left( \frac{dH}{H} - \frac{dp}{p} + \frac{dp_v^*}{p_v^*} \right). \tag{2}$$

This relationship allows one to diagnose relative changes of  $\gamma_d$  from the observed changes in pressure, temperature (which controls  $p_v^*$ ) and relative humidity. Since  $\gamma \equiv p_v/p \sim 10^{-2} \ll 1$ , we can assume  $\gamma = \gamma_d$  and neglect  $\gamma$  in the right-hand side of Eq. (2).

Table 1: Available estimates of mean precipitation  $\overline{P}$ , evaporation  $\overline{E}$  and their ratio within an area of up to  $r$  from the center of tropical cyclones (ordered by increasing  $r$ ). Asterisks denote North Atlantic hurricanes.

Storm	$r$ (km)	$\overline{E}/\overline{P}$	$\overline{P}$ (mm h <sup>-1</sup> )	$\overline{E}$ (mm h <sup>-1</sup> )	Date	Ref.
*Helen	37	0.14	18	2.6	1958/09/26	1
Nari	50	0.055	22.3	1.22	2001/09/19	2
*Bonnie	70	0.05	17.5	0.88	1998/08/22	3
*Helen	74	0.14	18.6	2.6	1958/09/26	1
*Katrina	100	0.11	19.1	2.1	2005/08/28	4
*Ivan	100	0.078	13.4	1.04	2004/09/14	4
Fay	100	0.059			1998/08/15	5
Fay	100	0.33			1998/08/14	5
*Helen	111	0.17	13.9	2.4	1958/09/26	1
*Daisy	150	0.18	3.3	0.6	1958/08/27	6
*Daisy	150	0.12	8.6	1.0	1958/08/25	6
Nari	150	0.096	6.55	0.63	2001/09/19	2
*Bonnie	200	0.08	10.1	0.81	1998/08/22	3
Morakot	240	0.088	8.3	0.73	2009/08/07	7
Fay	300	0.17	1.4	0.24	1998/08/15	5
Fay	300	0.29	0.7	0.2	1998/08/14	5
*Katrina	400	0.26	4.3	1.1	2005/08/28	4
*Ivan	400	0.2	2.97	0.60	2004/09/14	4
Model cyclone	500	0.21	0.88	0.185		8
*Lili	700-900	0.52			2002/09/15-27	9
*Isidore	900-1300	0.47			2002/09/22-10/04	9

References: 1 – Miller (1962); 2 – Yang et al. (2011); 3 – Braun (2006); 4 – Trenberth et al. (2007); 5 – Fritz and Wang (2014); 6 – Riehl and Malkus (1961); 7 – Huang et al. (2014); 8 – Kurihara (1975); 9 – Jiang et al. (2008). Estimates provided by Hawkins and Rubsam (1968), Hawkins and Imbembo (1976) and Gamache et al. (1993) (0.3-0.5 for  $\overline{E}/\overline{P}$  for  $r \lesssim 100$  km) are not listed as they are considered to be overestimates (Braun, 2006).

If, as is commonly assumed, the temperature of the air parcel does not change (e.g., Emanuel, 1986), we have  $dp_v^*/p_v^* = 0$ . Using typical values of  $H$  and  $p$  from Fig. 1 we find

$$\frac{\Delta_{AB}\gamma}{\gamma_B} = \frac{H_B - H_A}{H_B} - \frac{p_B - p_A}{p_B} = 0.25. \quad (3)$$

As the air reaches the windwall, it ascends. If the ascending air reaches a sufficient height, as occurs in intense cyclones, it cools to such low temperatures that all water vapor

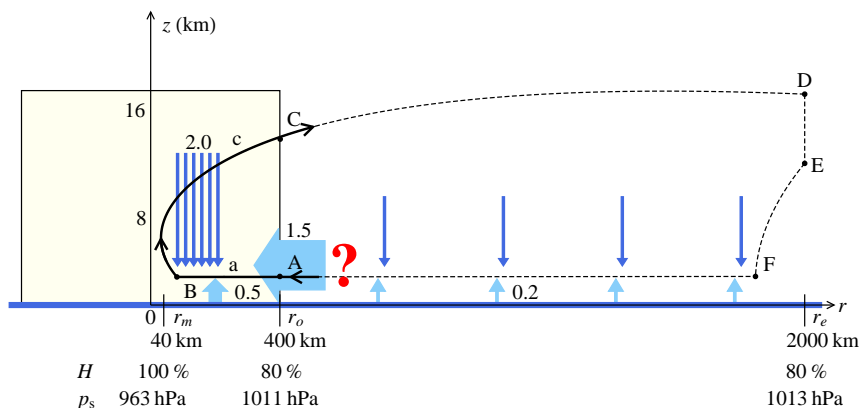


Figure 1: A scheme for hurricane water vapor budgets based on Table 1 and the data for 1551 observations of North Atlantic hurricanes in 1998-2015 (see Methods):  $r_m = 41 \pm 24$  km is the radius of the maximum wind velocity ( $\pm$  one standard deviation);  $r_o = 396 \pm 121$  km is the radius of the outermost closed isobar;  $r_e \sim 2000$  km is a distant radius representing the mean tropical environment;  $H$  and  $p_s$  are relative humidity and air pressure at the surface  $z = 0$ ; typical values for  $H$  at  $r_m$ ,  $r_o$  and  $r_e$  are shown (Holland, 1997) as well as  $p_s(0) = 963 \pm 19$  hPa,  $p_s(r_o) = 1011 \pm 3$  hPa and  $p_s(r_e) = 1013$  hPa as mean tropical sea level pressure. The box represents the hurricane, black arrows represent air streamlines. Values by upward blue arrows indicate typical mean evaporation ( $\text{mm h}^{-1}$ ) in the outer region  $r \geq r_o$  and the inner region  $r \leq r_o$  (1  $\text{mm h}^{-1}$  corresponds to 1  $\text{kg H}_2\text{O m}^{-2} \text{h}^{-1}$ ). Horizontal blue arrow: typical import of water vapor into the hurricane ( $1.5 \text{ mm h}^{-1}$  for  $r \leq r_o$ ). Downward arrows: mean rainfall within the inner area  $r \leq r_o$  equals  $2.0 \text{ mm h}^{-1}$  (import plus evaporation); on larger areas mean rainfall approaches mean evaporation (see text). Dashed streamlines and the question mark at the horizontal blue arrow indicate that the origin of imported moisture remains unknown.

condenses:  $\gamma_B \gg \gamma_C \approx 0$  (Fig. 1). Practically all this condensed moisture precipitates within the area  $r \leq r_o$  (Makarieva et al., 2013a; Huang et al., 2014; Braun, 2006). Thus, we have

$$\frac{\Delta_{BC}\gamma}{\gamma_B} = \frac{\gamma_C}{\gamma_B} - 1 \approx -1. \quad (4)$$

Thus, every air parcel entering the hurricane at point A and leaving it at point C (Fig. 1) acquires  $\Delta_{AB}\gamma$  moles of water vapor by evaporation from the ocean and loses  $-\Delta_{BC}\gamma$  moles of water vapor due to condensation and precipitation per each mole of dry air it contains. Therefore, for the ratio of the mean evaporation  $\overline{E}$  to mean precipitation  $\overline{P}$  within area  $r \leq r_C = r_A$  we have

$$\frac{\overline{E}}{\overline{P}} = -\frac{\Delta_{AB}\gamma}{\Delta_{BC}\gamma} = 0.25. \quad (5)$$

In intense real-world cyclones the air temperature near the oceanic surface is not constant but may decline towards the eyewall reflecting the rapid expansion of air parcels entering the area of lower pressure. For example, in hurricane Isabel the surface air temperature drops by  $-\Delta_{AB}T = 2$  K as the air approaches the windwall from the periphery (Montgomery et al., 2006). This corresponds to a negative third term in the right-hand part of Eq. (2) of the order of  $\Delta_{AB}p_v^*/p_v^* = (L/RT)\Delta_{AB}T/T \sim -0.12$  for  $T = 300$  K, where  $L = 45$  kJ mol<sup>-1</sup> is the latent heat of vaporization. In this case from Eq. (2) we have  $\Delta_{AB}\gamma/\gamma_B = 0.2 + 0.05 - 0.12 = 0.13$ . This means that 87% of moisture condensing within the hurricane must be imported from elsewhere. As Eq. (2) shows, if the temperature drop is just slightly larger and the relative humidity increase is slightly less than in our example above, the positive and negative terms in Eq. (2) may cancel yielding zero evaporation. In consequence, observational estimates of oceanic evaporation possess large uncertainties (see, e.g., Table 1 of Bell et al. (2012)).

Since no direct measurements of surface water vapor flows in tropical cyclones exist (Trenberth et al., 2003), available estimates of oceanic evaporation either rely on the same governing relationship (2) for various air streamlines (e.g., Bell et al., 2012) or consider the mass budget of the hurricane by comparing observed rainfall rates to estimates of imported moisture (Table 1). Moisture convergence can be estimated from the experimentally measured or modelled wind field around the cyclone. Using such estimates we can verify how Eq. (2) explains the observed relationships.

First, Eq. (2) predicts that in weak storms, where the air does not rise as high and associated condensation in the rising air is incomplete, we have  $-\Delta_{BC}\gamma < \gamma_B$ , and the evaporation-to-precipitation ratio (5) can grow. This pattern is reported for the tropical storm Fay (Fritz and Wang, 2014). At the initial stage of the storm development, rainfall within 300 km was 0.7 mm h<sup>-1</sup> and the estimated evaporation-to-rainfall ratio was 0.33 and 0.29 within 100 and 300 km, respectively (Fig. 2). As the storm intensified, rainfall within 300 km doubled, while  $\overline{E}/\overline{P}$  declined to 0.059 and 0.17 within 100 and 300 km, respectively (Table 1 and Fig. 2). Likewise, hurricane Daisy at higher rainfall had a smaller  $\overline{E}/\overline{P}$  than at lower (Table 1 and Fig. 2).

Second, Eq. (2) explains why  $\overline{E}/\overline{P}$  diminishes in the region  $r_m < r < r_o$  as compared to  $r > r_o$  (Fig. 2). This is because for  $r < r_o$  we only consider a certain part of the total pressure fall and relative humidity increment, while still accounting for most of condensation and precipitation which take place in the ascending air in a narrow zone near the windwall (consider path aBc in Fig. 1). In other words,  $\Delta_{aB}H$  and  $-\Delta_{aB}p$  are smaller than  $\Delta_{AB}H$  and  $-\Delta_{AB}$  in Eq. (3), while  $\gamma_c \approx \gamma_C$  and  $\Delta_{Bc}\gamma \approx \Delta_{BC}\gamma$ . Thus,  $-\Delta_{aB}\gamma/\Delta_{Bc}\gamma < -\Delta_{AB}\gamma/\Delta_{BC}\gamma$ , cf. Eq. (5). Therefore, for  $r < r_o$  we can observe small ratios  $\overline{E}/\overline{P} < 0.25$ . This agrees with the available estimates (Table 1 and Fig. 2).

In the vicinity of hurricane's center – in the hurricane's eye – the air descends and rainfall is absent. Thus, if evaporation is estimated from Eq. (2) for  $r < r_m$  (Fig. 1), it can locally exceed rainfall. This is illustrated by the available estimates of local oceanic evaporation in hurricanes Fabian and Isabel in 2003 (Bell et al., 2012). We calculated

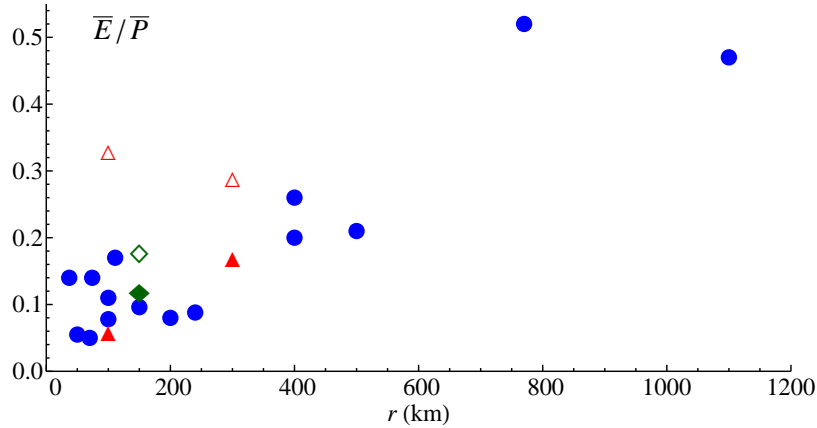


Figure 2: Available estimates of evaporation-to-rainfall ratio for tropical cyclones as dependent on distance  $r$  from the cyclone center;  $\bar{E}$  and  $\bar{P}$  are the mean evaporation and precipitation within a circle of radius  $r$ , respectively (Table 1). Empty and filled triangles: tropical storm Fay on 1998/08/14 (lower rainfall) and 1998/08/15 (higher rainfall), respectively. Empty and filled diamond: hurricane Daisy on 1958/08/27 (lower rainfall) and 1958/08/25 (higher rainfall), respectively. Circles – the remaining data from Table 1.

evaporation  $E$  from the data of Fig. 15 of Bell et al. (2012) on the oceanic enthalpy flux  $Q_O$  ( $\text{W m}^{-2}$ ) assuming that the evaporation latent heat flux accounts for three quarters of  $Q_O$ ,  $EL = 0.75Q_O$  (Jaimes et al., 2015), and using the conversion coefficient  $1 \text{ mm h}^{-1} = 696 \text{ W m}^{-2}$  (Trenberth et al., 2003). In these hurricanes the radius  $r_P$  of maximum precipitation, which we defined as the mean radius of the 10% highest rainfall values, is about twice the radius of maximum wind (Fig. 3). Thus, local estimates of evaporation can be close to or exceed local rainfall,  $E \approx P$  for  $r < r_P$  (see, e.g., Fig. 3e), while the mean ratio  $\bar{E}/\bar{P}$  within the area  $r < r_P$  can remain low.

Finally, Eqs. (2)-(5) do not provide support to the idea that the moisture imported into the hurricane at  $r < r_o$  derives from local evaporation in the region  $r > r_o$ . In this outer area neither surface pressure nor relative humidity change appreciably with  $r$  as compared to their changes within the hurricane (Fig. 1). Thus, as the air parcel moves along the surface towards the hurricane center (consider path FA in Fig. 1), it neither gathers nor loses water vapor, i.e. its  $\gamma$  does not change. This means that such an air parcel neither imports nor exports moisture to/from the oceanic area above which it is moving.

This means that for  $r > r_o$ , i.e. outside the area of considerable changes in surface pressure and humidity, locally evaporated moisture precipitates locally. Obviously, with  $r_o < r \rightarrow \infty$ , the evaporation-to-rainfall ratio should rise towards unity. Thus, for hurricanes Isidore and Lili the ratio assessed for  $r \sim 1000 \text{ km}$  is about 0.5 (Table 1 and Fig. 2).



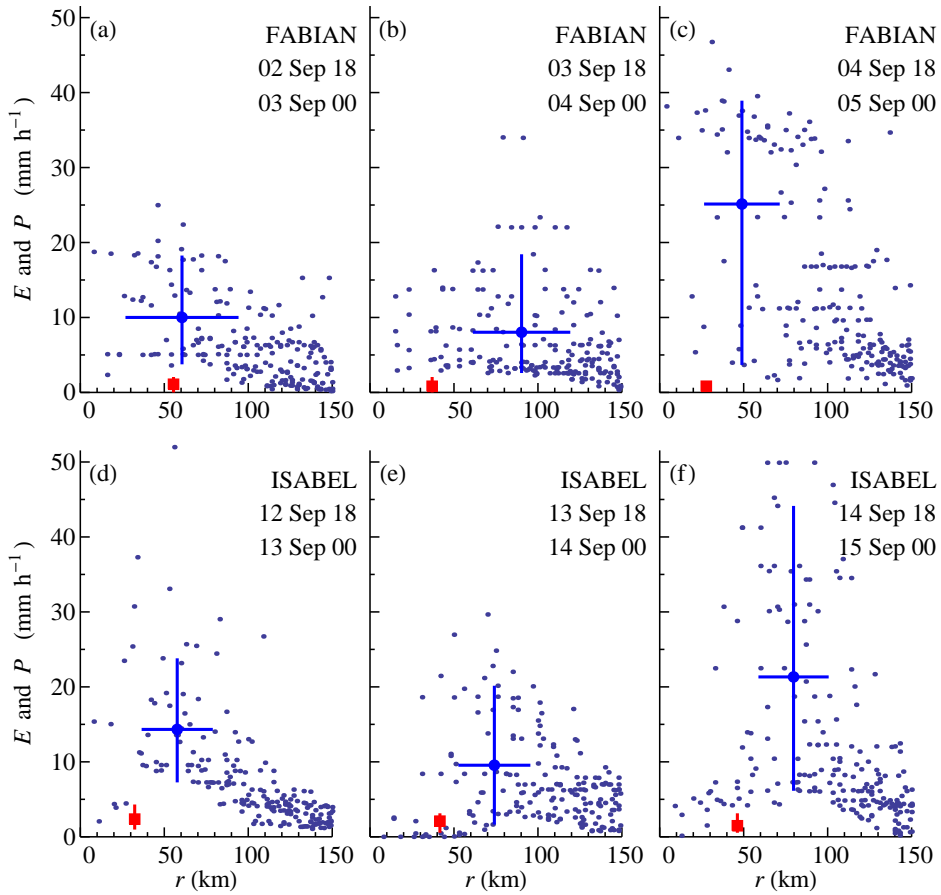


Figure 3: Local precipitation  $P$  and evaporation  $E$  versus distance  $r$  to the hurricane’s center in hurricanes Fabian (a-c) and Isabel (d-f) (see Methods for details). The dots show rainfall in individual grid cells of the TRMM dataset. Date and time (UTC) are for the two EBTRK positions closest to the measurements of Bell et al. (2012, see their Fig. 5). The big circles are the mean  $P$  for  $r_P - \Delta r_P \leq r \leq r_P + \Delta r_P$ , where  $\Delta r_P$  is the standard deviation of radius  $r_P$  of maximum precipitation. The horizontal lines at the circles correspond to  $r_P \pm \Delta r_P$ , the vertical lines connect the lower and upper 10% quantiles of  $P$ . The vertical red lines show the full range of  $E$  estimates from Fig. 15 of Bell et al. (2012) and the red squares are their mean values.

If not from evaporation that occurs over the ocean simultaneously with the hurricane development, how does the hurricane get moisture to sustain its rainfall?



### 3 Methods

We used the "extended best track" dataset (EBTRK) released 27 July 2016 (Demuth et al., 2006). We picked up all observations in 1998-2015 of Atlantic tropical cyclones with maximum velocity  $V_{\max} > 34 \text{ m s}^{-1}$  (hurricanes) south of  $40^\circ \text{ N}$ , a total of 1551 observations for 122 different storms. Mean radii of maximum wind  $r_m$  and outermost closed isobar  $r_o$ , mean sea level pressure in hurricane's center and at  $r = r_o$  were calculated from EBTRK data (Fig. 1). Translation velocity  $V_c$ , i.e. velocity at which the cyclone center moves relative to the Earth's surface, was calculated for each observation as the distance between the current and next position of the hurricane's center divided by six hours (EBTRK data are recorded every six hours). The average translation velocity was  $V_c = (5.9 \pm 2.9) \text{ m s}^{-1}$  ( $\pm$  standard deviation).

We used 3-hourly TRMM 3B42 (version 7) and 1-hourly MERRA MAI1NXINT datasets to calculate local rainfall  $P(r)$  ( $\text{mm h}^{-1}$ ) and total water vapor in the atmospheric column  $\sigma(r)$  ( $\text{mm}$ ) depending on distance  $r$  from the hurricane's center. Local values  $P(r_i)$  and  $\sigma(r_i)$  were defined as the mean rainfall and water vapor content in all grid cells with  $r_{i-1} \leq r < r_i$ ,  $1 \leq i \leq 120$ ,  $r_i \equiv 25 \times i \text{ km}$ ,  $r_0 \equiv 0 \text{ km}$ ,  $r_{120} = 3000 \text{ km}$ .

Tropical rainfall and atmospheric moisture vary significantly in space and time. Hurricanes, too, happen at different time of the year in different parts of the Atlantic ocean. To distinguish the hurricanes' moisture footprint from regional, seasonal and diurnal variability we introduced reference functions  $X_0(r)$ ,  $X = \{P, \sigma\}$ . They were calculated as the mean value of the considered variable for those seventeen years in the eighteen years' 1998-2015 period when the hurricane *did not happen*.

For each data entry we also calculated the same variables three days before and three days after the hurricane, denoting them, respectively,  $X^-$  and  $X^+$  ( $X = \{P, \sigma, P_0, \sigma_0\}$ ).

For example, for hurricane Isabel observed 2010/09/13 at 18 UTC at  $22.5^\circ \text{ N } 62.1^\circ \text{ W}$  (EBTRK data entry AL1303) we calculated the dependence of rainfall  $P$  on distance  $r$  from this point on 13 September at 18 UTC in all years except 2010. The mean of the obtained seventeen  $P(r)$  dependencies was defined as  $P_0(r)$ . Variable  $P_0^+(r)$  describes the dependence of rainfall on distance  $r$  from the same point ( $22.5^\circ \text{ N } 62.1^\circ \text{ W}$ ) on 16 September at 18 UTC (three days after the hurricane) averaged over all years, 1998-2015, except 2010. Variable  $\sigma^-(r)$  describes the dependence of local atmospheric moisture content on distance  $r$  from the same point ( $22.5^\circ \text{ N } 62.1^\circ \text{ W}$ ) on 10 September 2010 at 18 UTC (three days before the hurricane).

Finally, for all introduced variables  $X = \{P, P^\pm, \sigma, \sigma^\pm, P_0, P_0^\pm, \sigma_0, \sigma_0^\pm\}$  we calculated  $\overline{X}(r) \equiv 2\pi \int_0^r X(r')r'dr'/\pi r^2$ . Everywhere below the overbar  $\overline{X}(r)$  denotes the average of the considered variable  $X(r)$  in the circle of radius  $r$ . Variables without overbars,  $X(r)$ , correspond to mean values at a distance  $r$  from the hurricane's center. Subscript "0" denotes reference variables calculated in hurricane absence to describe an average hurricane-free environment.

Thus, for each of the 1551 analyzed EBTRK data entries we obtained twenty four

functions –  $P(r)$ ,  $\overline{P}(r)$ ,  $\sigma(r)$ ,  $\overline{\sigma}(r)$ ,  $P_0(r)$ ,  $\overline{P}_0(r)$ ,  $\sigma_0(r)$ ,  $\overline{\sigma}_0(r)$ ,  $P^\pm(r)$ ,  $\overline{P}^\pm(r)$ ,  $\sigma^\pm(r)$ ,  $\overline{\sigma}^\pm(r)$ ,  $P_0^\pm(r)$ ,  $\overline{P}_0^\pm(r)$ ,  $\sigma_0^\pm(r)$ ,  $\overline{\sigma}_0^\pm(r)$ . Their values averaged for each  $r$  over all analyzed EBTRK data entries are shown in Figs. 4 and 5.

The spatial resolution of the TRMM and MERRA datasets are  $0.25^\circ$  latitude  $\times$   $0.25^\circ$  longitude and  $0.5^\circ$  latitude  $\times$   $0.67^\circ$  longitude, respectively. Since rainfall is highly non-uniform spatially and temporally, rainfall observations in a single TRMM grid cell are characterized by high uncertainty. For example, for most grid cells with zero rainfall rate the error is  $0.35 \text{ mm h}^{-1}$ ; for grid cells with a high rainfall rate the error is usually several times the rate itself. Thus, a reliable rainfall estimate demands at least a hundred observations.

The standard error for a given  $r$  of the rainfall variables averaged across all analyzed EBTRK data entries (Fig. 5) was calculated following Huffman (1997) as  $s_P(r) = \sqrt{\sum_{i=1}^{n(r)} s_i^2 / n(r)}$ . Here  $s_i$  is the error of the  $i$ -th rainfall value as recorded in the TRMM dataset and  $n(r)$  is the total number of TRMM rainfall values analyzed for a given  $r$  for a given variable:  $n(r) = \sum_{j=1}^{mN_h} k_j$ , where  $N_h = 1551$ ,  $m = 17$  for variables corresponding to hurricane absence (17 years) and  $m = 1$  otherwise, and  $k_j \geq 0$  is the number of rainfall values for a given  $r$  for the  $j$ -th observation (here "observation" is a unique combination of coordinate, date and time).

Compared to rainfall, the atmospheric water vapor content is a much less variable quantity. We estimated the standard error of the water vapor variables as  $s_\sigma(r) = \beta(r) / \sqrt{N_h(r)}$ , where  $\beta(r)$  is the standard deviation of  $N_h(r)$  values of the considered variable for a given  $r$ ;  $N_h(r) \leq 1551$  is the number of hurricane observations for each  $r$ .

For the water vapor variables for some hurricanes the data were missing for  $r \leq 75 \text{ km}$ , which is close to the spatial resolution of the MERRA dataset. The minimum number of data analyzed was  $N_h(r) = 817$  for  $r = 25 \text{ km}$ , with each hurricane observation represented by one  $\sigma(r)$  value. The number of data for a given  $r$  for each hurricane observation increases with growing  $r$  and is larger for the spatially averaged variables  $\overline{X}(r)$  compared to local variables  $X(r)$ . For  $r = 300 \text{ km}$  the mean number of values analyzed for each hurricane observation was  $13 \pm 3$  and  $90 \pm 6$  for  $\sigma(r)$  and  $\overline{\sigma}(r)$  and  $70 \pm 5$  and  $478 \pm 30$  for  $P(r)$  and  $\overline{P}(r)$  ( $\pm$  one standard deviation), with totals of, respectively, 20471, 138966, 109279 and 740759. Our main results pertain to  $300 \text{ km} < r < 1500 \text{ km}$ .

## 4 Hurricane's long-range moisture signatures

### 4.1 Hurricane's dry footprint

We begin with discussing reference functions  $\sigma_0(r)$  and  $P_0(r)$  which characterize the hurricane region in hurricane absence. In those years when hurricanes do not happen, the atmospheric water vapor content  $\sigma_0(r)$  declines with increasing distance  $r$  from the hypothetical hurricane center. Its maximum and minimum values,  $\sigma_0(r) = 42.6 \pm 0.006 \text{ mm}$

at  $r = 75$  km and minimum  $\sigma_0(r) = 35.8 \pm 0.001$  mm at  $r = 3000$  km ( $\pm$  one standard error), differ by 19% (Fig. 4a,d). This reflects the steeper temperature gradients and lower temperatures associated with large  $r$  at higher latitudes. A similar although less regular pattern is found for local reference rainfall: maximum  $P_0(r) = 0.202 \pm 0.005$  mm h<sup>-1</sup> and minimum  $P_0(r) = 0.171 \pm 0.001$  mm h<sup>-1</sup> for  $r = 100$  km and  $r = 2650$  km, respectively, differ by 18% (Fig. 5a,d). In the absence of moisture import across  $r = 3000$  km (the largest radius considered in this study), the long-term mean spatially averaged rainfall  $\overline{P}(r)$  for  $r \leq 3000$  km equals the long-term mean oceanic evaporation  $E_0$  in the hurricane region,  $E_0 = \overline{P}_0(3000 \text{ km}) = 0.182 \pm 0.0001$  mm h<sup>-1</sup>.

In the presence of hurricanes the water vapor content is higher,  $\sigma(r) > \sigma_0(r)$  for  $r < 10^3$  km. This difference is due, at least in part, to the re-distribution of water vapor within the hurricane. Because of the rapid vertical ascent of air near the eyewall  $r \sim r_m$  (Fig. 1), this region is saturated with water vapor, so  $\sigma(r)$  rises for small  $r$ . At larger  $r$ , however, a slightly higher  $\sigma(r)$  may reflect the fact that hurricane wind speeds *preferentially develop* when and where the amount of water vapor is larger than usual. This is confirmed by the fact that water vapor content three days before the hurricane,  $\sigma^-(r)$ , is on average higher than it is three days after the hurricane and than it is in hurricane absence, i.e.  $\sigma^-(r) > \sigma^+(r) \approx \sigma_0(r)$  (Fig. 4c,f). The maximum difference  $\sigma^-(r) - \sigma^+(r) = 1.5$  mm is reached for  $r = 700$  km, where  $\sigma^-(r) = 43.1 \pm 0.04$  mm,  $\sigma^+(r) = 41.6 \pm 0.04$  mm and  $\sigma_0(r) = 41.9 \pm 0.03$  mm (Fig. 4c). During the hurricane the moisture content at this radius rises to  $\sigma(r) = 44.0 \pm 0.03$  mm (Fig. 4a).

Dry air expelled from the hurricane should descend somewhere thus suppressing rainfall and diminishing moisture content outside the hurricane. Indeed, we find that in the presence of hurricanes, local rainfall  $P(r)$  displays a remarkable behavior: it is higher than  $P_0(r)$  for  $r < r_d = 625$  km and lower than  $P_0(r)$  for  $r \geq r_d$ , Fig. 5a. (A qualitatively similar behavior, albeit at larger radii, is displayed by local water vapor content in the presence of hurricanes  $\sigma(r)$ , Fig. 4a.) The minimum is reached at  $r = 1050$  km; here  $P(r) = 0.12 \pm 0.004$  mm h<sup>-1</sup> is only 60% of  $P_0(r) = 0.19 \pm 0.001$  mm h<sup>-1</sup>.

The existence of this minimum is supported by the fact that local rainfall in the hurricane center three days before and three days after the hurricane,  $P^-(r)$  and  $P^+(r)$ , declines considerably below the long-term mean  $P_0(r)$ , Fig. 5c. A hurricane moving with translation velocity  $V_c = 6$  m s<sup>-1</sup> covers about 1.5 thousand kilometers in three days. Thus, according to Fig. 5a, the point which in three days from now becomes a new hurricane center is currently located within the region of minimal rainfall of the approaching hurricane (see Fig. 5c). Therefore, rainfall in the considered point three days before the hurricane is lower than the long-term mean,  $P^-(0) < P_0(0)$ . (Indeed, Anthes (1974) noted that "one of the earliest recognized signs of an approaching storm is the unusual suppression of normal tropical cloudiness". Figure 5c quantifies this effect.) For the same reason the rainfall three days after the hurricane declines as well,  $P^+(0) < P_0(0)$ , Fig. 5c.

This rainfall minimum for  $r > r_d$  is not just a property of the statistical mean precip-

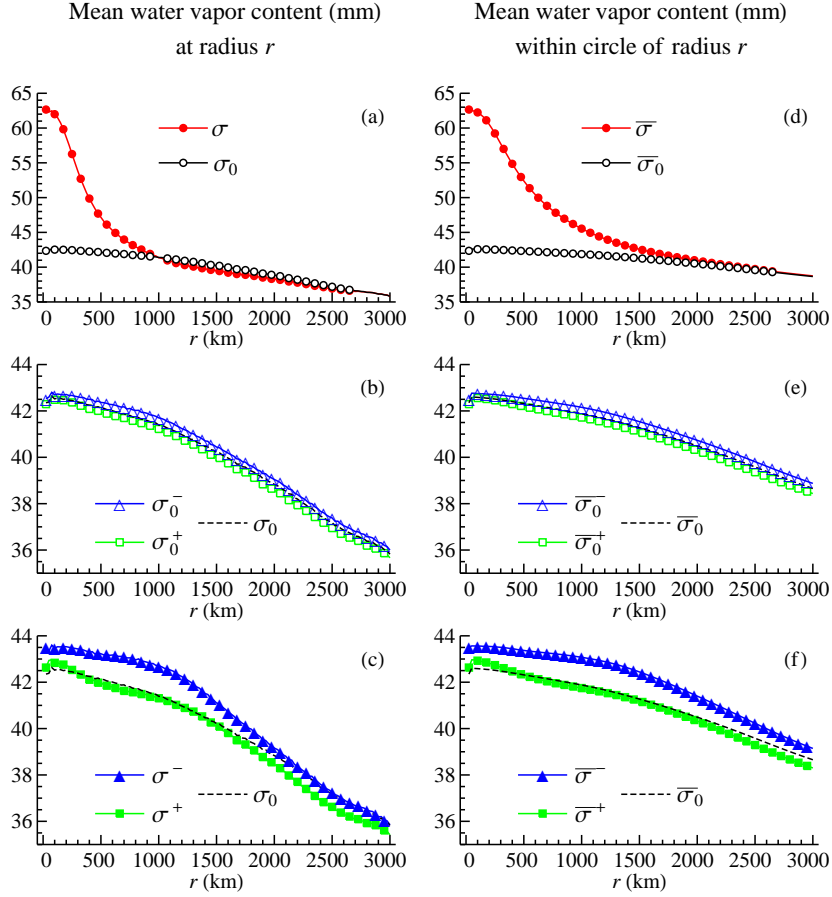


Figure 4: Mean water vapor content versus radial distance  $r$  from a hurricane's center for 1551 observations of North Atlantic hurricanes in 1998-2015 (see Methods for the description of variables). (a)-(c) mean water vapor content at radius  $r$ ; (d)-(f) mean water content within circle of radius  $r$  (variables with overbars). Filled symbols and empty symbols (variables with subscript 0) correspond to the presence and absence of hurricanes, respectively. Superscripts "−" and "+" correspond to the water vapor distribution three days before and three days after the hurricane, respectively. In each panel, the pair of solid curves lacks symbols at those  $r$  where the difference between the two variables is less than twice the sum of their standard errors (see Methods).

itation distribution averaged over all hurricane observations (Fig. 5a). In every hurricane there is a region  $r > r_d$  where rainfall  $P(r)$  drops to values below the long-term mean rainfall  $P_0(r)$  and long-term mean evaporation  $E_0$ , although the magnitude of this drop and its precise location vary from hurricane to hurricane (Fig. 6).

For each hurricane observation, we defined  $r_d \geq r_m$  as the minimal radius where

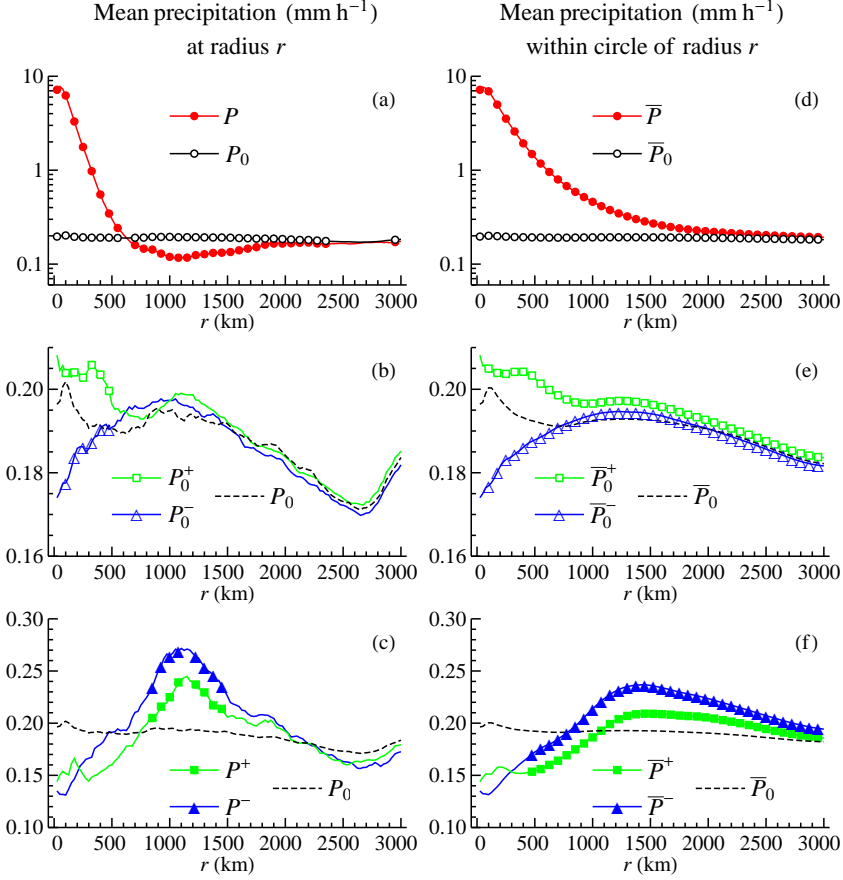


Figure 5: Same as in Fig. 4 but for rainfall rate. Note the logarithmic scale on the vertical axis in (a) and (d). The two precipitation maxima in (c) are an indication of where the hurricane center is on average located – relative to the current hurricane position – three days before and three days after the hurricane.

$P(r_d) = E_0 = 0.18 \text{ mm h}^{-1}$  ( $r_m$  is the radius of maximum wind, Fig. 1). For 1545 observations where  $r_m$  is known in the EBTRK dataset, we obtained  $r_d = 502 \pm 230 \text{ km}$  ( $\pm$  one standard deviation). This is lower than  $r_d = 625 \text{ km}$  estimated from the average rainfall distribution in Fig. 5a. We can call  $r_d \approx 500 \text{ km}$  the radius of the "dry footprint" left by the hurricane in its wake: within the circle  $r \leq r_d$  hurricane rainfall  $P(r)$  rises above the long-term mean tropical oceanic evaporation.

The mean radius where minimum rainfall is observed for each hurricane observation for  $r \geq r_m$  was  $r_{\min} = 1206 \pm 725 \text{ km}$ , which is larger than  $r_{\min} = 1050 \text{ km}$  estimated from the average rainfall distribution in Fig. 5a. The mean minimal rainfall was  $P_{\min}(r_{\min}) = 0.011 \pm 0.15 \text{ mm h}^{-1}$ , in good agreement with the above discussed minimum of  $P(r)$  in

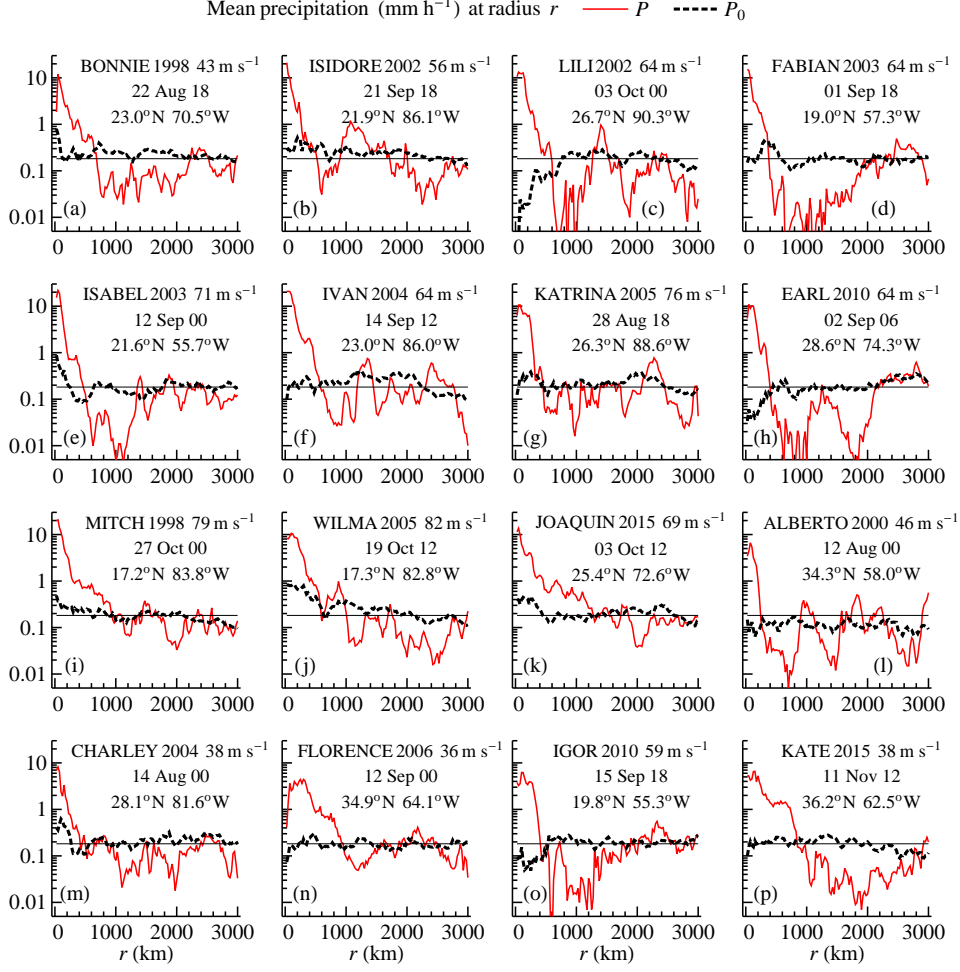


Figure 6: Precipitation versus distance from the hurricane center in some North Atlantic hurricanes: (a)-(h) eight hurricanes discussed in Section 2: Bonnie, Ivan, Katrina, Isidore, Lili (Table 1), Fabian, Isabel (Fig. 3), Earl (Jaimes et al., 2015); (i)-(k) three most intense hurricanes in 1998-2015 (one most intense hurricane in each six years is chosen), (m)-(p) ( $n \times 310$ )th ( $n = 1, 2, 3, 4, 5$ ) from our set of  $5 \times 310 + 1 = 1551$  analyzed observations (ordered by date) as examples of randomly selected hurricanes. As in Fig. 5a,  $P(r)$  is the actual rainfall distribution in the hurricane,  $P_0(r)$  is the rainfall distribution in those seventeen years when the hurricane did not occur (see Methods). Horizontal line denotes  $E_0 = \overline{P_0}(3000 \text{ km}) = 0.18 \text{ mm h}^{-1}$  from Fig. 5d. Maximum wind velocity, the date and time of the observation and the coordinate of the hurricane center  $r = 0$  are from the EBTRK dataset.

Fig. 5a. The frequency distributions of  $r_d$  and  $r_{\min}$  show that in most hurricanes local rainfall falls below the long-term mean evaporation between  $300 \text{ km} < r \leq 500 \text{ km}$ , while

the minimum rainfall is observed within  $600 \text{ km} < r \leq 900 \text{ km}$  (Fig. 7).

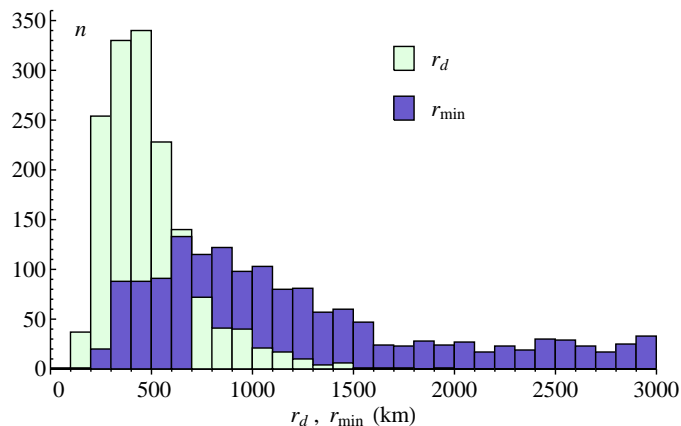


Figure 7: Frequency distribution of  $r_d \geq r_m$ , for which  $P(r_d) = E_0 = 0.18 \text{ mm h}^{-1}$ , and  $r_{\min} \geq r_m$ , for which  $P(r_{\min})$  is minimal, for 1545 hurricane observations.

## 4.2 Rainfall and evaporation

In contrast to local rainfall  $P(r)$ , which is either lower or higher than  $P_0(r)$  depending on  $r$ , mean rainfall  $\bar{P}(r)$  within a circle of radius  $r$  is always higher in the presence of hurricanes than in their absence,  $\bar{P}(r) \geq \bar{P}_0(r)$  for  $r \geq 0 \text{ km}$  (Fig. 5d). This has important implications for understanding a hurricane’s water vapor budget.

Previous studies suggested that a hurricane can be sustained by evaporation on an area of a three-five times larger radius than that of hurricane’s rainfall area (Anthes, 1974; Trenberth et al., 2003). In the framework of our results, the rationale behind such a statement can be formulated as follows. Within a hurricane of radius  $r_o = 400 \text{ km}$  mean rainfall rate  $\bar{P}(r_o) = 1.9 \text{ mm h}^{-1} = 1.9 \text{ kg H}_2\text{O m}^{-2} \text{ h}^{-1}$  is over ten times the long-term mean evaporation  $E_0 = 0.18 \text{ mm h}^{-1}$ . Total hurricane rainfall ( $\text{kg H}_2\text{O h}^{-1}$ ) equals  $\Pi \equiv \pi r_o^2 \bar{P}(r_o)$ . This rainfall can be generated by the steady-state mean evaporation within an area  $r \leq r_e$ , where  $r_e$  is determined by the equality  $\Pi = \pi r_e^2 E_0$ . This gives  $r_e = r_o \sqrt{\bar{P}(r_o)/E_0} = 1300 \text{ km}$ .

However, this mass-balance consideration presumes that all water vapor produced by evaporation on a larger area  $r \leq r_e$  is concentrated to precipitate within the inner circle  $r \leq r_o < r_e$ . Then there is no rainfall in the ring  $r_o \leq r \leq r_e$ . In reality we have seen that mean local rainfall  $P(r)$ , while reduced at larger radii, never falls below 60% of  $E_0$  (Fig. 5a). According to our analysis, mean local rainfall for  $400 \text{ km} \leq r \leq 3000 \text{ km}$  is  $0.89E_0$ . This means that only 11% of water vapor evaporated outside the hurricane could have been imported into the inner circle  $r \leq r_o$ . Thus, the necessary



radius which could ensure the observed rainfall distribution within  $r \leq r_o$  rises up to  $r_e \approx r_o \sqrt{\bar{P}(r_o)/E_0/0.11} \approx 3900$  km. There is no evidence that concentration of moisture at this scale – an area of nearly eight thousand kilometers in diameter – occurs.

We also note that the observed suppression of rainfall for  $r \geq r_d$  does not necessarily imply that a certain part of evaporated moisture is exported from this area to the inner hurricane area. Rather, this is an indication of dry air masses expelled from the hurricane descending outside and mixing with local air. This would suppress local rainfall and allow water vapor to accumulate in the atmosphere after its depletion by the cyclone. Frank (1977), based on observations for northwest Pacific cyclones, indicated that around 440–660 km from the cyclone center there is a region of air subsidence throughout most of the troposphere. This radius is close to radius  $r_d$  of the hurricane’s dry footprint that we estimated at  $r_d \approx 500$  km in the previous section. It corresponds to the so-called *moat* of clear skies that typically surround tropical cyclones. It is at this radius that the water vapor drawn into the cyclone at the mid-level descends to the boundary layer to be driven towards the eyewall by the boundary layer inflow and then condense in the air updrafts (Frank, 1977).

For  $r = 1300, 2000$  and  $3000$  km we find that  $\bar{P}(r)$  is, respectively, 67%, 17% and 6% higher than the long-term evaporation  $E_0$ . Since long-term steady-state evaporation is limited by the available solar energy, these findings suggest that a hurricane is not a steady-state system in the sense that, while maintaining a high moisture content within itself (Fig. 4a), it depletes atmospheric moisture faster than it is replenished by evaporation on a scale of a few thousand kilometers. This is supported by the observation that moisture content prior to hurricane formation is appreciably higher than after the hurricane sweeps the area,  $\sigma^-(r) > \sigma^+(r)$  (Fig. 4c,f).

We will now propose a distinct concept regarding how atmospheric moisture sustains a hurricane. In this concept there is no need to draw in moisture over thousands of kilometers but rain is sustained from atmospheric stocks within about 700 km of the storm’s center.

## 5 Water vapor budget and hurricane movement

### 5.1 Governing relationships

Can a hurricane sustain itself through its motion? A hurricane of diameter  $2r$  moving through the atmosphere with velocity  $U$  sweeps an area of  $S = 2rU\Delta t$  during a time interval  $\Delta t$  (Fig. 8). The total amount of water vapor in this area in a hurricane-free environment is  $2rU\Delta t\sigma_0(r)$ . Let all this moisture condense and precipitate within the hurricane area  $\pi r^2$  during same time interval. Mean rainfall in the circle of radius  $r$  ( $\text{mm h}^{-1}$ ) will be

$$\bar{P}_m(r) = \frac{2rU\Delta t\sigma_0(r)}{\pi r^2\Delta t} = \frac{U}{\pi r} 2\sigma_0(r). \quad (6)$$

In the frame of reference co-moving with the storm, the import of water vapor into the hurricane corresponds to mean radial velocity  $V_r = U/\pi$ : water vapor flux captured by the hurricane's diameter  $2r$  is averaged over circumference of length  $2\pi r$ . Water vapor leaves the hurricane via rainfall over area  $\pi r^2$ . So factor  $2/r$  in Eq. (6) is the consequence of the continuity equation (matter conservation).

Note that  $\overline{P}_m(r)$  is the maximum rainfall for a given  $r$  available to the hurricane through its motion. This upper limit is reached if all water vapor encountered by the hurricane over a distance of  $2r$  is used up (condensed and precipitated) within it. In other words, a non-zero velocity  $U > 0$  is a necessary but insufficient condition for a hurricane to sustain its rainfall by motion. If the air flows through the hurricane without losing moisture or if the air blows around the hurricane without entering it, the motion-related rainfall can be zero however large  $U$ . In such a case  $U > 0$  but  $V_r = 0$  (see thin air streamlines in Fig. 8b).

Putting  $U = V_c$  in Eq. (6), where  $V_c = 5.9 \text{ m s}^{-1}$  is the mean translation velocity of our hurricanes, and using  $\sigma_0(r)$  from Fig. 4a in Eq. (6), we find that motion-related rainfall  $\overline{P}_m(r)$  equals observed rainfall  $\overline{P}(r)$  for  $r = r_h = 700 \text{ km}$  (Fig. 9). This means that water vapor available in an average hurricane-free environment is sufficient to generate the observed hurricane rainfall within a circle of  $r_h = 700 \text{ km}$  radius *even if evaporation for  $r \leq r_h$  is zero*. We can say that radius  $r_h$  is the radius of a hurricane's self-sufficiency with respect to water vapor: as long as the hurricane moves through the atmosphere with velocity  $U$  equal to translation velocity and consumes all ambient vapor it encounters, its rainfall is sustained. Such a hurricane does not need to concentrate moisture from afar.

For  $100 \text{ km} \geq r < r_h \text{ km}$  the observed rainfall  $\overline{P}(r)$  is higher than the motion-related rainfall  $\overline{P}_m(r)$  by up to 55% (Fig. 9). This reflects the radial concentration of the incoming moisture within the moving hurricane. The radial velocity  $V_r$  that delivers water vapor to the inner area  $r < r_h$  may increase with diminishing  $r$  from its mean value of  $V_r = U/\pi$  at  $r = r_h$  to over twenty meters per second at its maximum in the vicinity of the windwall (Trenberth et al., 2003; Montgomery et al., 2006; Makarieva and Gorshkov, 2011). This concentration causes local rainfall  $P(r)$  at  $r < r_c$  to rise above the mean rainfall  $\overline{P}(r_h)$ , while at larger radii it remains lower. Radius  $r_c = 375 \text{ km}$ , where  $P(r_c) = \overline{P}(r_h)$ , appears to be close to the radius of the outermost closed isobar,  $r_c \approx r_o = 400 \text{ km}$  (Fig. 9). The ring  $r_c = r_o \leq r \leq r_h$  serves as the donor of water vapor for the inner circle  $r \leq r_c = r_o$ . The spatial scales linking water budgets and pressure/velocity distributions merit further investigations.

Real hurricanes would move through the atmosphere and obtain water vapor by motion more slowly,  $U < V_c$ . On the other hand, evaporation within  $r \leq r_h$ , however small, is not zero. These factors, as we show below, compensate each other such that the basic scenario we have just considered turns out to produce a realistic self-sufficiency radius  $r_h \approx 700 \text{ km}$ .

Expressing  $U$  in terms of translation velocity as  $U \equiv k_U V_c$ , we define *available rainfall*  $\overline{P}_a(r)$  within a circle of radius  $r$  as the sum of rainfall due to motion and rainfall due to

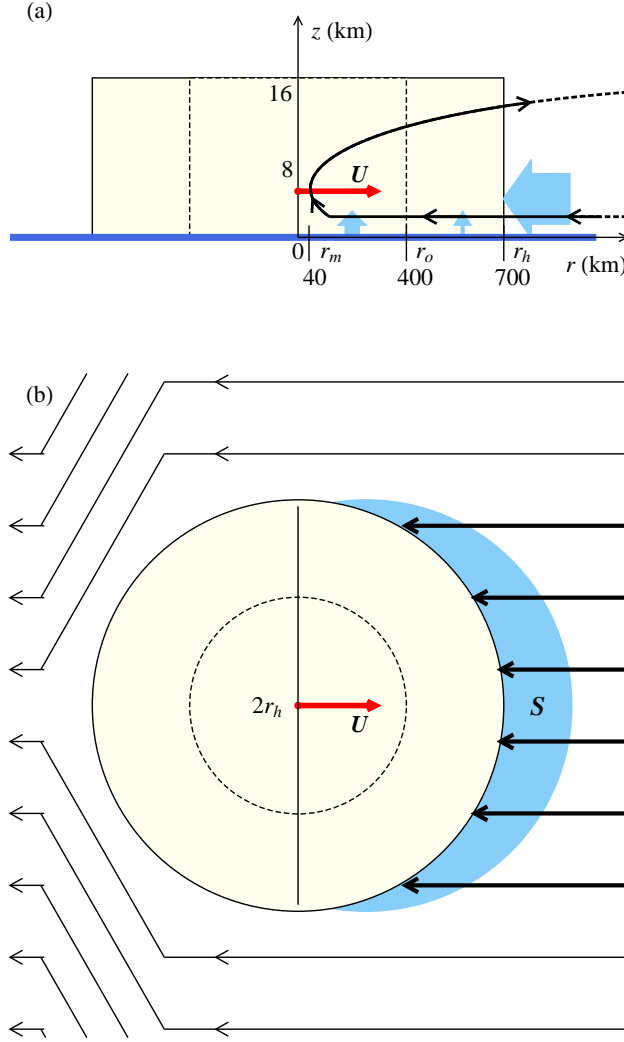


Figure 8: (a) Water vapor budget in the hurricane rest frame (cf. Fig. 1). As the hurricane moves through the atmosphere with velocity  $U$  relative to the ambient air, it consumes the ambient water vapor. Dry air leaving the hurricane in the upper atmosphere does not return. (b) A bird's-eye view of (a) from the top of the inflow layer:  $S = 2r_h U \Delta t$  is the area swept by the hurricane's diameter  $2r_h$  in time  $\Delta t$ . Water vapor in the inflow layer on area  $S$  is drawn into the hurricane, condenses and precipitates during the time interval  $\Delta t$ . Thick air streamlines are those that bring in moisture and disappear within the hurricane (the air ascends and leaves the hurricane above the inflow layer). Thin streamlines show air flowing around the hurricane without entering it.

evaporation that is concurrent with the hurricane:

$$\bar{P}_a(r) = k_\sigma \bar{P}_m + k_E E_0 = k \frac{V_c}{\pi} \frac{2}{r} \sigma_0(r) + k_E E_0, \quad (7)$$

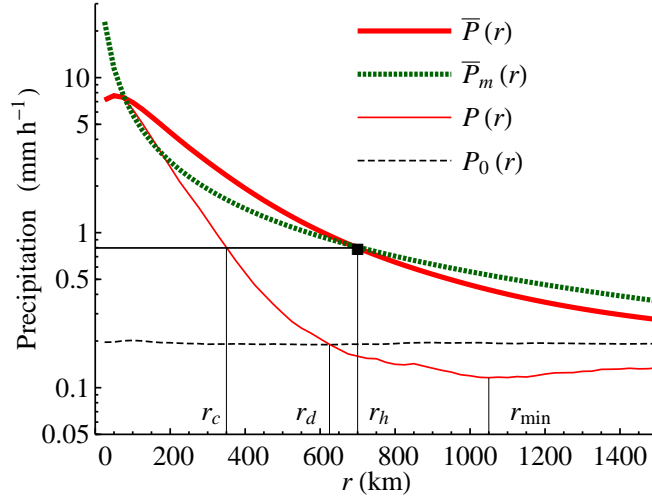


Figure 9: Motion-related rainfall  $\overline{P}_m(r)$  versus observed rainfall  $\overline{P}(r)$  for  $U = V_c$  in Eq. (6). Local rainfall  $P(r)$  and reference rainfall  $P_0(r)$  from Fig. 5a are also shown to illustrate the relationship between the inner radius  $r_d$  of the hurricane's "dry footprint", for which  $P(r_d) = P_0(r_d)$ , the self-sufficiency radius  $r_h$ , for which  $\overline{P}(r_h) = \overline{P}_m(r_h)$ , and the characteristic radius  $r_c$  of water vapor re-distribution within the hurricane, for which  $P(r_c) = \overline{P}(r_h)$  (see text for details).

where  $k \equiv k_\sigma k_U$ . Coefficient  $k_\sigma \leq 1$  in Eq. (7) describes how completely the hurricane uses up the store  $\sigma_0(r)$  of atmospheric water vapor that it encounters. Long-term evaporation  $E_0 = 0.18 \text{ mm h}^{-1}$  does not depend on hurricane motion. Coefficient  $k_E(r) \geq 0$  describes how evaporation in hurricane presence varies relative to the long-term mean;  $\overline{E}(r) = k_E(r)E_0$  is the mean evaporation within the circle of radius  $r$ .

Before comparing available rainfall to observations we discuss  $k_U$ ,  $k_\sigma$  and  $k_E$  in Eq. (7).

## 5.2 Key parameters

### 5.2.1 Thickness of the inflow layer

The value of  $k_\sigma \leq 1$  describes the effective thickness of the inflow layer, where the hurricane takes in the ambient water vapor (Fig. 8a):

$$k_\sigma(z) \equiv \frac{\sigma(z, r)}{\sigma_0(r)}, \quad \sigma(z, r) \equiv \int_0^z q(z', r) \rho(z', r) dz'. \quad (8)$$

Here  $q = \rho_v/\rho$  is absolute humidity (mass fraction of water vapor) (Fig. 10a),  $\rho$  is air density and  $\rho_v$  is water vapor density,  $\sigma(z)$  is the amount of water vapor vapor below altitude  $z$  (Fig. 10b) and  $\sigma_0$  is the total amount of water vapor in the atmospheric column.

Since air temperature declines with height, the vertical distribution of water vapor is bottom-heavy: the warmer lower 7 km of the tropical atmosphere contain over 95% of total water vapor in the atmospheric column (Fig. 10c). We have  $k_\sigma(z) = 1$  if the inflow layer of height  $z$  harbors all water vapor in the atmospheric column.

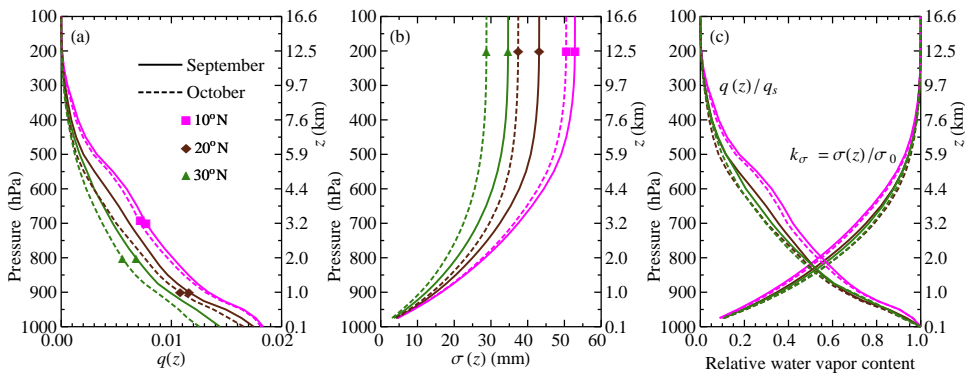


Figure 10: Zonally averaged water vapor content as derived from the monthly MERRA dataset MAIMCPASM for 2015: Absolute values of  $q(z)$  (a) and  $\sigma(z)$  (b), see Eq. (8), in September and October (the months accounting for two thirds of all hurricane observations in our analysis) at 10°, 20° and 30° N; (c) same functions as in (a) and (b) but each divided by its respective value at 1000 hPa for  $q(z)$  (subscript  $s$ ) and at 0.1 hPa for  $\sigma(z)$  (subscript 0).

The inflow into the cyclone in the region  $r > r_o = 400$  km occurs up to the level of 400-500 hPa or about 7 km – in contrast to the smaller radii where the inflow is confined to the lowest one and a half kilometer (Miller, 1958; Frank, 1977; Montgomery et al., 2006). At a given  $r$  this inflow appears to be stronger in hurricanes than it is on average in tropical cyclones (Fig. 11a, solid line). Frank (1977) emphasized the importance of this mid-level inflow for the energy budget of tropical cyclones. Most of this inflow should subside to the boundary layer ”before being cycled upwards in clouds” at smaller radii (Frank, 1977).

The outflow in intense cyclones occurs above 10 km (Fig. 11a). The air expelled by the hurricane is nearly completely dry, because at these heights water vapor content diminishes to negligible magnitudes of the order of  $\gamma \sim 10^{-5}$  (Fig. 10a). This corresponds to  $\gamma_C = 0$  in Fig. 1. Thus, a cyclone where the inflow occurs in the lower 7 km and outflow occurs above 10 km can suck in and use up practically all atmospheric water vapor it encounters, i.e. for it  $k_\sigma \approx 1$  in Eq. (7). If the inflow occurs in the lower three kilometers, then  $k_\sigma \approx 0.7$  (Fig. 10c).

The ratio of  $\sigma(z)/\sigma_0$  is practically independent of  $\sigma_0$  (cf. Fig. 10b and 10c). This justifies our consideration of  $k_\sigma$  (8) as a function of  $z$  only.

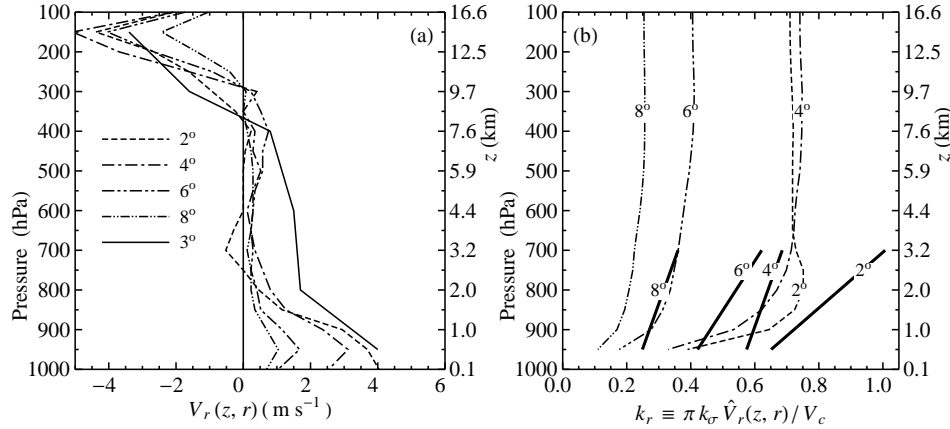


Figure 11: Radial velocity  $V_r$  versus height  $z$  at selected radial distances  $r$  (shown in degrees latitude). (a) data for  $2^\circ$ ,  $4^\circ$ ,  $6^\circ$  and  $8^\circ$  are from Fig. 12 of Frank (1977) for Northwest Pacific tropical cyclones; data for  $3^\circ$  – from Fig. 9 of Miller (1958) for North Atlantic hurricanes; (b)  $k_r \equiv \pi k_\sigma \hat{V}_r(z, r)/V_c$  (see Eqs. 10 and 12) for  $V_c = 5.7 \text{ m s}^{-1}$ ; dashed curves – data of Frank (1977) from (c); solid curves – data from Fig. 8 of Miller (1958) for Atlantic hurricanes.

### 5.2.2 Propagation velocity $U$

Velocity  $U$  in Eqs. (6) and (7) would be equal to the translation velocity  $V_c$  of the cyclone, i.e. to the velocity at which the cyclone center moves relative to the Earth’s surface, if the storm moved through an otherwise still atmosphere. When the hurricane is embedded into an air flow, velocity  $U$  is equal to the difference between translation velocity  $V_c$  and mean velocity  $V_e$  of environmental flow. This velocity is sometimes referred to as *propagation velocity* (Carr III and Elsberry, 1990; Franklin et al., 1996). Propagation velocity  $\mathbf{U}(r)$  at a given radius is equal to translation velocity  $\mathbf{V}_c$  minus mean velocity  $\mathbf{V}_e(r)$  of air contained within a narrow ring  $r, r + dr$ :  $\mathbf{U}(r) = \mathbf{V}_c - \mathbf{V}_e(r)$ .

Propagation velocity has been studied in the context of the *steering flow* concept, whereby the tropical cyclone motion is considered as driven by the surrounding air flow (George and Gray, 1976; Chan and Gray, 1982; Holland, 1984; Dong and Neumann, 1986; Carr III and Elsberry, 1990; Franklin et al., 1996; Chan, 2005; Yasunaga et al., 2016). Propagation velocity is non-zero when the cyclone deviates from the steering flow. Previous studies focused on finding a horizontal scale and a pressure level where this deviation is minimized – such that translation velocity  $\mathbf{V}_c$  (and thus cyclone track) could be predicted from velocity  $\mathbf{V}_e$  of the ambient air (George and Gray, 1976; Holland, 1984; Franklin et al., 1996).

There are few studies where variation in local values of  $U$  with height and distance from the cyclone center would be systematically assessed. The limited available evidence indicates that propagation velocity  $U = k_U V_c$  increases with distance from the hurricane

center. At 200-300 km from the center  $U$  is about  $1.5\text{-}2 \text{ m s}^{-1}$ , or about one third of a typical translation velocity  $V_c$ . It approaches or even exceeds  $V_c$  at  $r \sim 1000 \text{ km}$  (Fig. 12a). This indicates that near its center the hurricane moves as a relatively rigid system: for small  $r$  the ring  $r, r + dr$  moves at approximately the same mean velocity as the storm's inner circle. With growing radial distance the storm's becomes less "rigid": the inner hurricane parts begin to move relative to the surroundings with a considerable velocity. Another feature is a maximum of  $U$  at the surface as compared to the mid troposphere (Fig. 12a).

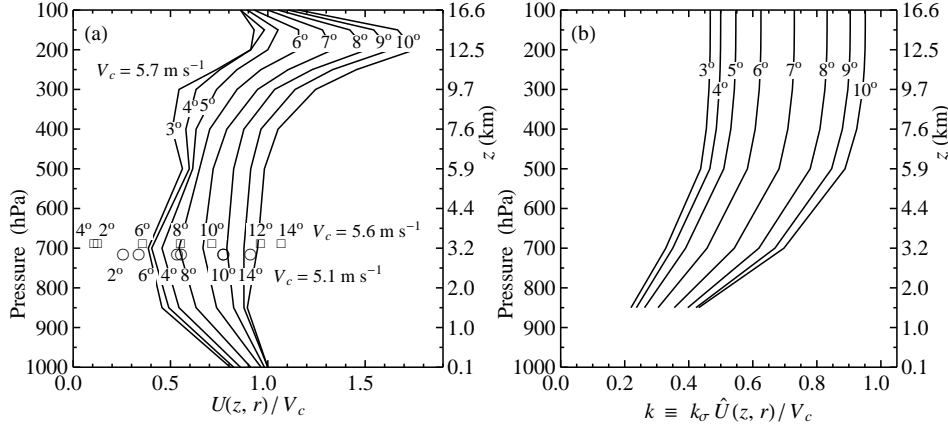


Figure 12: Propagation velocity versus height  $z$  at selected radial distances  $r$  (shown in degrees latitude). (a) Ratio of propagation velocity to translation velocity  $U(z, r)/V_c$ , solid curves – data from Table 3 of Franklin et al. (1996) for Atlantic tropical cyclones; symbols at 700 hPa – data from Figs. 12 and 13 of George and Gray (1976) for North Pacific tropical cyclones to the north (squares) and to the south (circles) of  $20^\circ \text{ N}$ ; (b)  $k \equiv k_\sigma k_U$  (see Eq. 11) for Atlantic cyclones from (a).

Mean propagation velocity  $\hat{U}$  and radial velocity  $\hat{V}_r$  in the inflow layer of height  $z$  (weighted by water vapor content  $q\rho$ , see Eq. 8) are

$$\hat{U}(z, r) = \frac{\int_0^z U(z', r) q(z', r) \rho(z', r) dz'}{\sigma(z, r)}, \quad (9)$$

$$\hat{V}_r(z, r) = \frac{\int_0^z V(z', r) q(z', r) \rho(z', r) dz'}{\sigma(z, r)}, \quad (10)$$

where  $\sigma(z, r)$  is given by Eq. (8).

For coefficient  $k$  in Eq. (7) using Eqs. (8) and (9) we have

$$k(z, r) \equiv k_U(z, r) k_\sigma(z) = \frac{\hat{U}(z, r) \sigma(z, r)}{V_c \sigma_0(r)}, \quad k_U(z, r) \equiv \frac{\hat{U}(z, r)}{V_c}. \quad (11)$$



Using the available data on  $U$  (Fig. 12a) and  $k_\sigma$  (Fig. 10c) we find that  $k(z, r)$  varies from 0.2 to unity for  $300 \text{ km} \lesssim r \lesssim 1100 \text{ km}$  and  $1.5 \text{ km} \lesssim z \lesssim 17 \text{ km}$  (Fig. 12b). For a given radial distance there is little change of  $k$  above 400 hPa, where  $k$  reaches its maximum. This reflects the absence of water vapor in the upper atmosphere – whatever flows in or out of the hurricane above 400 hPa does not affect its moisture budget.

As we discussed in Section 5.1, at the radius where the hurricane actually takes in the ambient water vapor, mean radial velocity in the inflow layer should be related to propagation velocity as  $\hat{V}_r = \hat{U}/\pi$ . At this radius  $k(z, r)$  (11) should coincide with  $k_r(z, r)$  defined as

$$k_r(z, r) \equiv \pi \frac{\hat{V}_r(z, r)}{V_c} k_\sigma = \pi \frac{\hat{V}_r(z, r)}{V_c} \frac{\sigma(z, r)}{\sigma_0(r)}. \quad (12)$$

Figure 11b shows that for  $200 \text{ km} \lesssim r \lesssim 900 \text{ km}$  and  $1.5 \text{ km} \lesssim z \lesssim 17 \text{ km}$  we have  $0.1 \leq k_r(r, z) \leq 1$ . Where  $k_r(z, r)$  and  $k(z, r)$  actually coincide is discussed below (see Section 5.3). We note that  $q(z)$  and  $\sigma(z)$  used to calculate  $k_r$  and  $k$  in Figs. 11b and 11c correspond to  $20^\circ\text{N}$  in September (see Fig. 10b). Using other months and/or latitudes does not affect the resulting values of  $k_r$  and  $k$  because of the approximate independence of  $q(z)/q_s$  and  $k_\sigma = \sigma(z)/\sigma_0$  of, respectively,  $q_s$  and  $\sigma_0$  (Fig. 10c).

### 5.2.3 Evaporation

To specify coefficient  $k_E$  that describes the input of evaporation into hurricane rainfall in Eq. (7), we take into account the observed rainfall distribution  $\bar{P}(r)$  (Fig. 5d). Mean precipitation within a circle of  $r_o = 400 \text{ km}$  is  $1.9 \text{ mm h}^{-1}$ , or about ten times the long-term evaporation mean,  $\bar{P}(r_o) = 10E_0$  (Fig. 13). On the other hand, according to Table 1 and in agreement with Eq. (5), we have  $\bar{E}(r_o)/\bar{P}(r_o) = 0.25$ . Thus, we have  $\bar{E}(r_o) = 2.5E_0$ . This means that evaporation within the outermost closed isobar of the hurricane on average exceeds the long-term mean by two and a half times:

$$k_E = \begin{cases} k_{E1}, & \text{if } r \leq r_o \\ k_{E2} + (k_{E1} - k_{E2}) \left(\frac{r_o}{r}\right)^2, & \text{if } r > r_o \end{cases} \quad (13)$$

where  $r_o = 400 \text{ km}$ ,  $k_{E1} = 2.5$  and  $k_{E2} = 1$ .

Outside the outermost closed isobar,  $r > r_o$ , local evaporation is assumed to be equal to its long-term mean,  $E(r) = k_{E2}E_0$ ,  $k_{E2} = 1$ . Then mean evaporation for  $r > r_o$  is given by  $\bar{E}(r) \equiv k_E(r)E_0 = [k_{E1}E_0\pi r_o^2 + k_{E2}E_0\pi(r^2 - r_o^2)]/\pi r^2$ , which is Eq. (14). Relationship (14) captures the growth of evaporation-to-rainfall ratio with increasing  $r$  (Fig. 13). For  $r = 1000 \text{ km}$  we have  $\bar{E}(r)/\bar{P}(r) \sim 0.5$  in agreement with the results of Jiang et al. (2008) for Isidore (Table 1, Fig. 2). Equation (13) may not be valid for  $r \ll r_o$ , but our results to be obtained will pertain to larger  $r > r_o$ .

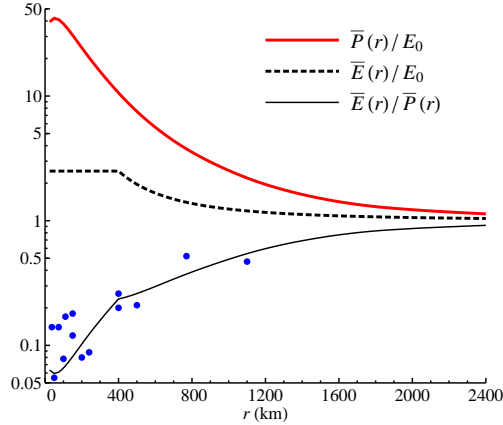


Figure 13: Observed rainfall  $\overline{P}(r)$  (Fig. 5d), evaporation  $\overline{E}(r) = k_E(r)E_0$  given by Eqs. (13)-(14) with  $k_{E1} = 2.5$  and  $k_{E2} = 1$ ), both in units of long-term evaporation  $E_0 = 0.18 \text{ mm h}^{-1}$ , and their ratio versus radial distance  $r$  from hurricane center. Circles are  $\overline{E}/\overline{P}$  ratios for North Atlantic hurricanes from Table 1.

### 5.3 Observational evidence

We can now compare available and observed rainfall,  $\overline{P}_a(r)$  (Eq. 7) and  $\overline{P}(r)$  (Fig. 5d). We varied  $k$  in Eq. (7) from 0.2 to 1 (as per Fig. 12b). For each  $k$ , for each  $r$ , for each out of our 1551 hurricane observations we used its translation velocity  $V_c$  calculated from the EBTRK dataset and its water vapor distribution  $\sigma_0(r)$  calculated from the MERRA dataset (see Methods and Fig. 4a). Putting these values into Eq. (7) with  $k_E$  given by Eqs. (13)-(14) we obtained available rainfall  $\overline{P}_a(r)$ . Available versus observed rainfall in selected hurricanes is shown in Fig. 14.

We compared available and observed rainfall in our set of 1551 hurricane observations in two ways. First, we averaged  $\overline{P}_a(r)$  and  $\overline{P}(r)$  separately and then found  $r = r_h$  where the two mean distributions coincide (Fig. 15a). Second, we averaged the ratio  $\overline{P}_a(r)/\overline{P}(r)$  for a given  $r$  and found the maximum  $r = r_h$  for which the mean ratio equals unity (Fig. 15b). The first way yields a higher  $r_h$  value; both values are reported below as the range of  $r_h$  estimates for each  $k$ .

We find that the self-sufficiency radius  $r_h$  grows with declining  $k$  (Fig. 16). Indeed, the value of  $k$  reflects how fast the hurricane moves relative to the ambient air and how much of the available water vapor it uses up (Eq. 11). Thus, with decreasing  $k$  available rainfall  $\overline{P}_a(r)$  becomes smaller at all  $r$ , including  $r = r_h$ . Since observed rainfall  $\overline{P}(r)$  declines with increasing  $r$ , the now smaller  $\overline{P}_a$  can equal  $\overline{P}$  at a larger  $r$  only. So  $r_h$  is larger for a smaller  $k$ .

The minimum value of  $r_h(k) = r_{h \text{ min}}$  is constrained by the dependence of  $k$  on  $r$  (Fig. 16). Since propagation velocity grows with increasing  $r$  (Fig. 12a), so does  $k(r)$ .

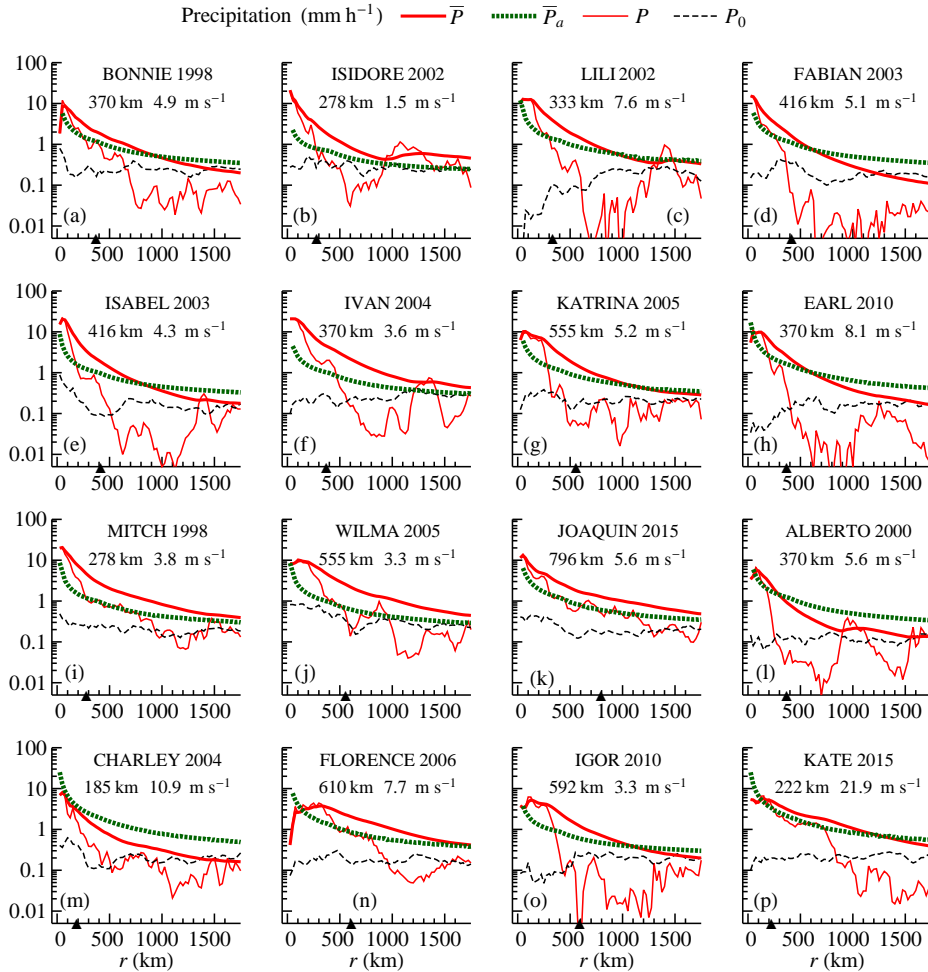


Figure 14: Observed  $\bar{P}(r)$  versus available  $\bar{P}_a(r)$  precipitation for  $k = 0.5$ ,  $k_{E1} = 2.5$  and  $k_{E2} = 1$  in Eqs. (7)-(14) for the same hurricanes as in Fig. 6, cf. Fig. 15a. Radius  $r_o$  of the outermost closed isobar (marked with triangle on the horizontal axis) and translation velocity  $V_c$  are from the EBTRK dataset.

Thus, while for  $k \rightarrow 1$  we find small values of  $r_h$ , these solutions are unrealistic: they would require too large propagation velocities at small radii. Realistic solutions are defined by the intersection of the curves  $k(r)$  and  $r_h(k)$  in Fig. 16. Since for any given  $r$  the maximum value of  $k(r)$  corresponds to the inflow layer of 400 hPa (Fig. 12b), we conclude that the minimum value of  $r_h$  is  $r_{h \min} = 670$  km corresponding to the intersection between  $k(r)$  for 400 hPa and the range of solutions  $r_h(k)$  (Fig. 16). If the inflow layer is thinner and does not reach up to 400 hPa, then minimal  $r_h$  increases; for an inflow layer below 850 hPa  $r_h$  must exceed 900 km (Fig. 16).

Since, as we discussed in Section 5.1,  $\bar{P}_a(r)$  only gives the upper limit of rainfall

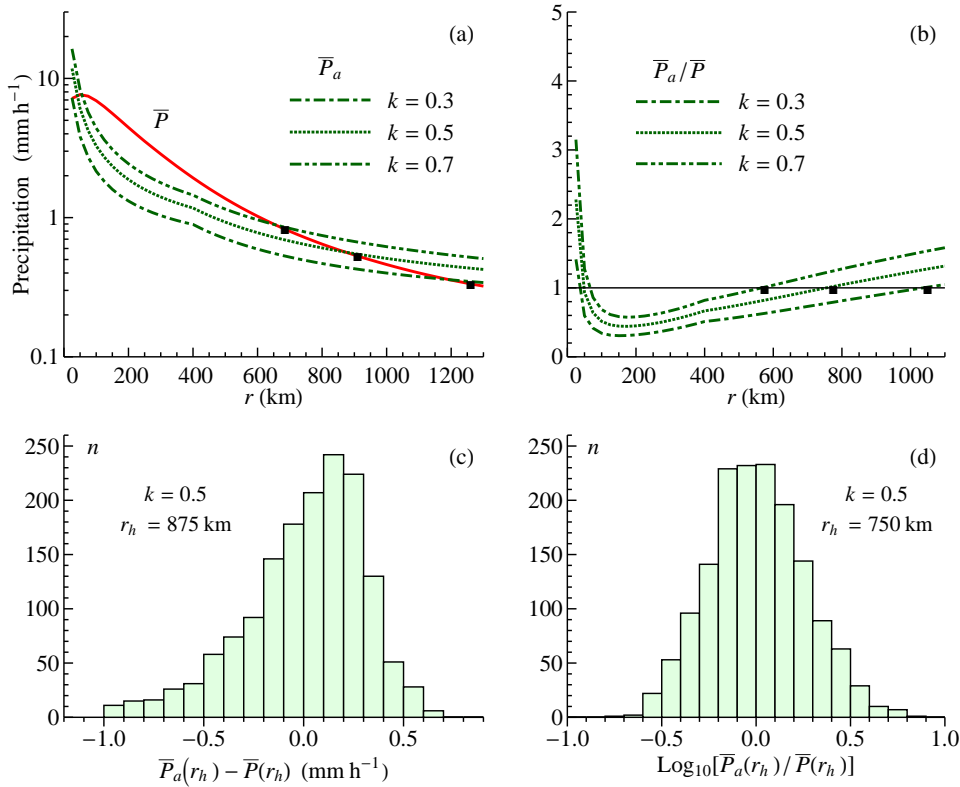


Figure 15: Available versus observed precipitation for selected  $k$  in Eq. (7). (a) Mean  $\overline{P}_a(r)$  ( $\text{mm h}^{-1}$ ) averaged for each  $r$  over all hurricane observations as compared to mean observed precipitation  $\overline{P}(r)$  ( $\text{mm h}^{-1}$ ) (see Fig. 5d). (b) Mean ratio  $\overline{P}_a(r)/\overline{P}(r)$  averaged for each  $r$  over all hurricane observations (log-normal distribution assumed). (c,d) Frequency distribution of  $\overline{P}_a(r_h) - \overline{P}(r_h)$  (mean  $\pm$  one standard deviation  $0.0016 \pm 0.87 \text{ mm h}^{-1}$ ) in (c) and  $\overline{P}_a(r_h)/\overline{P}(r_h)$  ( $0.0063 \pm 0.25$ ) in (d) for  $r_h$  corresponding to  $k = 0.5$ . Filled squares in (a) and (b) indicate radius of self-sufficiency  $r_h$  for each  $k$ .

available through motion, it is essential to find out whether the hurricanes actually take in the moisture they sweep by their diameter  $2r_h$ . If they do, mean radial velocity  $\hat{V}_r(r)$  at  $r = r_h$  must equal  $\hat{U}(r)/\pi$ . This requires that three curves,  $k_r(z, r)$  (Eq. 12),  $k(z, r)$  (Eq. 11) and  $r_h(k)$  must intersect at one point in Fig. 16. They do indeed: for the inflow layer below 700 hPa ( $z \approx 3 \text{ km}$ ) we find that  $k(r)$  and  $k_r(r)$  intersect at  $r = 750 \text{ km}$ . Here  $k(r) = k_r(r) = 0.5$ , which falls within the interval of estimated  $r_h(k)$  for  $k = 0.5$ . Since above 700 hPa the value of  $k_r(r)$  grows little (see Fig. 12b), it follows from Fig. 16 that there can be additional solutions for deeper inflow layers ( $z \geq 3 \text{ km}$ ) that correspond to  $r_{h \text{ min}} \leq r_h < 750 \text{ km}$ .

A hurricane's water budget can viewed as follows. At  $r = r_h \approx 700 \text{ km}$  the hurricane's

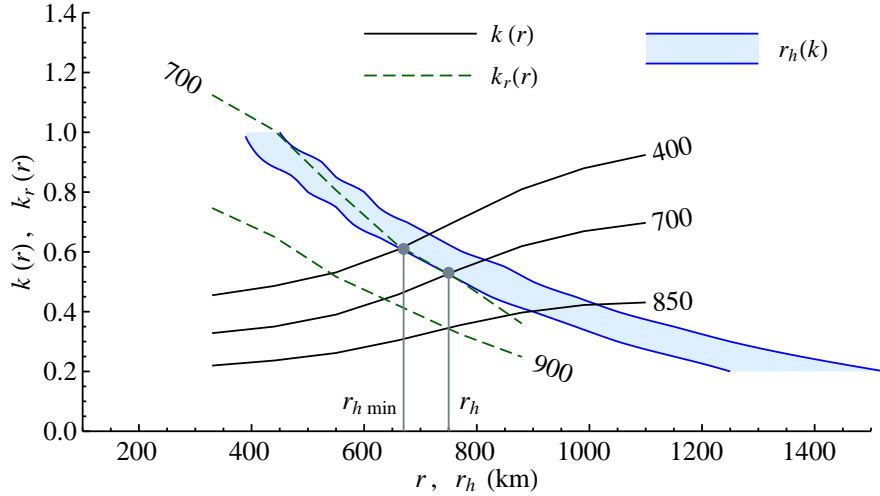


Figure 16: Self-sufficiency radius  $r_h$  versus parameter  $k$  in Eq. (7) (see text for details) and parameters  $k$  (Eq. (11), data from Fig. 12b) and  $k_r$  (Eq. (12), data from Fig. 11b of Miller (1958) for Atlantic hurricanes) versus radial distance  $r$ . Figures at curves denote height of the inflow layer in hPa.

inflow layer is at least  $z_i = 3$  km thick (up to 700 hPa). This inflow contains about 70% of the total moisture content in the atmospheric column: we have  $k_\sigma = 0.7$  in Eq. (7) (see Eq. (8) and Fig. 10c). The hurricane’s mean propagation velocity in the inflow layer is about 70% of its translation velocity:  $k_U = \hat{U}(z_i, r_h)/V_c = 0.7$  (Eq. 9). (Note that  $k_U$  and  $k_\sigma$  have coincided by chance as  $k = k_U k_\sigma = 0.5$  in Fig. 16; they are generally independent parameters.) Mean radial velocity  $\hat{V}_r$  at  $r = r_h$  is related to propagation velocity as  $\hat{V}_r = \hat{U}/\pi$ , which indicates that all water vapor the hurricane acquires by motion in the inflow layer actually condenses and precipitates within it. Thus, moving through the atmosphere with propagation velocity  $\hat{U} = 0.7V_c$  and consuming all water vapor it encounters in the lower 3 km, such a hurricane can sustain its rain observed within the circle  $r \leq r_h = 700$  km. Mean rainfall within area  $r \leq r_h$  is about four times the long-term mean (Fig. 9).

## 6 Hurricane water vapor budget and efficiency

The question of how the hurricane gathers its fuel – water vapor – is important for finding constraints on hurricane power and for predicting hurricane frequency. We have established that hurricanes can sustain rainfall by consuming *pre-existing* atmospheric moisture and leaving the atmosphere drier than it was before the hurricane (Fig. 4c,f). We now consider how this view relates to the commonly held alternative view of hurricanes as steady-state thermodynamic systems that consume heat and moisture from the ocean

(Emanuel, 1986, 1991; Ozawa and Shimokawa, 2015; Kieu, 2015).

Kinetic power  $W_K$  ( $\text{W m}^{-2}$ ) per unit hurricane area is commonly estimated as  $W_K = \rho C_D V^3$ , where  $V$  is air velocity and  $C_D \sim 2 \times 10^{-3}$  is surface exchange coefficient (Emanuel, 1999). Viewing hurricane as a heat engine consuming heat flux  $Q_O$  from the ocean, its maximum kinetic power is estimated as

$$W_K = \rho C_D V^3 = \varepsilon_C Q_O, \quad \varepsilon_C \equiv \frac{\Delta T}{T_s}, \quad (15)$$

where  $\varepsilon_C$  is Carnot efficiency,  $T_s$  is surface temperature,  $\Delta T \equiv T_s - T_{out}$ ,  $T_{out}$  is the minimum temperature of hurricane air in the upper atmosphere (Ozawa and Shimokawa, 2015). For  $T_s \approx 300$  K and  $\Delta T$  between 75 K and 105 K (DeMaria and Kaplan, 1994) we have on average  $\varepsilon_C = 0.3$ .

In the above analysis the assumption that heat influx  $Q_O$  occurs concurrently with the hurricane is crucial. This is because in theory the Carnot cycle efficiency relates heat input to work (J); it does not relate heat influx to power output ( $\text{J s}^{-1}$ ). To obtain power from work a characteristic time  $\tau$  of the considered thermodynamic cycle must be known. If heat input and kinetic energy production in the hurricane occur at the same time scale  $\tau_Q = \tau_W$ , i.e. concurrently, then hurricane power  $W_K$  can be constrained by Carnot efficiency (Eq. 15). If, on the other hand, heat input occurs on a much longer time scale than kinetic energy production in the hurricane,  $\tau_Q \gg \tau_W$ , then Eq. (15) will constrain the *mean kinetic energy production rate* observed during time  $\tau_Q$ . This mean rate will be by a factor of  $\tau_W/\tau_Q \ll 1$  smaller than the actual kinetic power output in a hurricane rendering Eq. (15) irrelevant.

An alternative approach is to consider the partial pressure of water vapor  $p_v$  ( $\text{J m}^{-3}$ ) as a store of potential energy equal to  $p_v/N_v = RT$  ( $\text{J mol}^{-1}$ ) (Makarieva and Gorshkov, 2009, 2011; Makarieva et al., 2010, 2013b). This energy is released when water vapor condenses, which can occur at an arbitrarily high rate proportional to the vertical velocity of the ascending air. Since potential energy can be converted to kinetic energy with efficiency equal to unity, this approach predicts that kinetic power output is proportional to rainfall:

$$W_K = \overline{P}RT, \quad (16)$$

where  $\overline{P}$  ( $\text{mol H}_2\text{O m}^{-2} \text{ s}^{-1}$ ) is mean rainfall within the hurricane and  $T$  is the mean temperature of condensation (Makarieva and Gorshkov, 2011).

And, indeed, Eq. (16) explains the observed average dependence of maximum velocity  $V_{\max}$  on rainfall in cyclones with  $V_{\max} \geq 30 \text{ m s}^{-1}$  (Makarieva et al., 2015a). On the other hand, the Carnot cycle view on hurricanes would be able to persist – as it does – only if Eq. (15) agreed with observations at least for some of the most intense hurricanes. How can the two alternative approaches give similar results?

Assuming that evaporation accounts for three quarters of total heat influx from the

ocean (Jaimes et al., 2015) we have for  $Q_O$  in Eq. (15)

$$Q_O = \frac{4}{3}\overline{E}L, \quad (17)$$

where  $L = 45 \text{ kJ mol}^{-1}$  is latent heat of evaporation.

Using Eq. (17) in Eq. (15) we observe that the two governing equations for the two alternative approaches, Eq. (15) and Eq. (16), would yield the same estimate of hurricane power  $W_K$  if

$$\frac{RT}{L} = \frac{4}{3}\frac{\overline{E}}{\overline{P}}\varepsilon_C. \quad (18)$$

It so happens that for intense hurricanes where  $\overline{E}/\overline{P}$  ratio is low, Eq. (18) is approximately fulfilled. For  $T \approx T_s - 15 \text{ K}$ ,  $T_s = 300 \text{ K}$ ,  $\varepsilon_C = 0.3$  and  $\overline{E}/\overline{P} = 0.13$  (as we estimated for hurricane Isabel in Section 2) we have

$$\frac{RT}{L} = 0.053 \approx \frac{4}{3}\frac{\overline{E}}{\overline{P}}\varepsilon_C = 0.052. \quad (19)$$

This analysis explains why, unlike Eq. (16), which is universally valid (Makarieva et al., 2015a), Eq. (15) can match observations only in intense hurricanes. In less intense storms, as we discussed in Section 2, condensation in the rising air is incomplete, and the evaporation-to-rainfall ratio in Eq. (19) increases. In the result, the right-hand part of the approximate equality in Eq. (19) exceeds  $RT/L$ . Thus, in less intense hurricanes with a larger evaporation-to-rainfall ratio, the Carnot constraint (15) does not match observations but should exceed the observed power (16). Conversely, one can predict that the actual hurricane power described by Eq. (16) can exceed the Carnot constraint (15) in those hurricanes where the evaporation-to-precipitation ratio is small. As we discussed in Section 2, this ratio should be small in those hurricanes where surface air temperature decreases towards the hurricane center – thus contributing a negative third term to the right-hand side of Eq. (2). Accordingly, it was hurricane Isabel where air temperature was dropping by 2 K as the air was approaching the windwall, that was reported to have exceeded the maximum potential intensity estimated from Eq. (15) (Montgomery et al., 2006).

We conclude that the approximate agreement between Eqs. (16) and (15) for intense hurricanes can be traced to an accidental numerical agreement between unrelated variables (Eq. 18). This coincidence explains how Eq. (15) can match selected observations despite hurricanes not in fact behaving as Carnot heat engines. Indeed, accounting for the atmospheric moisture source, the ratio between kinetic power and total latent heat flux  $Q_{in} = \overline{P}L$  is  $W_K/Q_{in} = RT/L \approx (1/5)\varepsilon_C \ll \varepsilon_C$ . It follows that the maximum observed hurricane power cannot be explained by viewing the hurricane as a thermodynamic cycle converting external heat to work at Carnot efficiency.



## 7 Conclusions

Most rainfall within the outermost closed isobar of a hurricane is due to imported moisture rather than local evaporation (Table 1 and Figs. 1 and 2). Here we have shown that while evaporation can be estimated from the observed radial distribution of pressure, relative humidity and temperature in the boundary layer, such estimates are insufficient to clarify the origin of imported moisture (Section 2).

We then considered rainfall and moisture distribution up to 3000 km from the hurricane center using TRMM and MERRA data. For each out of 1551 analyzed observations of North Atlantic hurricanes in 1998-2015 we defined reference distributions of rainfall and atmospheric moisture characterizing the hurricane environment in those years when the hurricane was absent. By comparing rainfall and moisture distributions in hurricanes to their seventeen years' hurricane-free means we established that hurricanes leave a dry footprint of suppressed rainfall in their wake. At distances  $r > r_d \sim 500$ -600 km from the center rainfall is reduced by up to 40% compared to what it is on average in hurricane's absence (Figs. 7 and 6). This pattern was not previously established in quantitative terms since most studies of hurricane-related rainfall focused on a smaller area of up to 300-400 km from the center (e.g., Lonfat et al., 2004). The inner radius  $r_d$  of hurricanes' dry footprint corresponds to the so-called clear sky moat that often surrounds tropical cyclones at 440-660 km from the storm's center (Frank, 1977).

We also showed that rainfall in hurricanes typically remains considerably larger than the sum mean evaporation up to 3000 km from the hurricane center. This indicates that a hurricane cannot be viewed as a steady-state system, whereby water vapor provided by *concurrent* evaporation across a few thousand kilometers could be concentrated to the smaller rainfall area of a hurricane (Section 4.2).

We offered a novel proposal for how hurricanes capture moisture: *pre-existing* atmospheric water vapor stores are consumed as the storm moves through the atmosphere. Rainfall available to the hurricane due to its movement is directly proportional to movement velocity  $U$  (Eq. 6). We found that radius  $r_h$  at which a moving hurricane becomes self-sufficient with respect to moisture is about  $r_h \sim 700$  km. This radius of self-sufficiency exceeds both the radius  $r_o \sim 400$  km of the uttermost closed isobar and the radius  $r_d \sim 500$ -600 km of hurricane's dry footprint:  $r_h > r_d > r_o$  (Fig. 9). This means that hurricane's movement provides for observed rainfall in the entire area  $r \leq r_d$  where the hurricane-related rainfall is elevated above the long-term mean characterizing a hurricane-free environment. Capturing its nearby water vapor by motion, such a hurricane does not need to concentrate moisture from far away.

In the present study we introduced general relationships and key parameters relating rainfall to motion. In particular, we proposed that propagation velocity  $U$ , i.e. storm's velocity relative to that of the surrounding air flow, is key for the cyclone's water vapor budget. So far propagation velocity has not been studied systematically as dependent on radial distance and altitude. Many studies focused on mean values of  $U$  for the entire

troposphere averaged across large radial distances (Chan, 2005). We noted that the cyclone’s water budget is determined by the mean value of  $U$  in the inflow layer at around  $r = r_h \sim 700$  km (Fig. 12b). This parameter, and especially its relationship to radial velocity (see Fig. 16 and Section 5.3), apparently merits more extensive investigations. For example, according to George and Gray (1976, see their Table 4), more intense cyclones appear to have a larger  $U$  than less intense ones. In our analysis the three most intense hurricanes have their available rainfall below observed rainfall at all  $r$  (Fig. 14i-k). These hurricanes also having a higher than average  $U$  could explain this pattern.

In our analysis we used the approximation of radial symmetry. However, cyclone motion relative to the ambient air must introduce asymmetries in the rainfall distribution. These are to be further investigated. According to Fig. 8, the rainfall asymmetry should be related to the direction of propagation velocity  $\mathbf{U}$  relative to the storm motion. The few available data indicate that in the lower layer of up to 700 hPa tropical cyclones move approximately colinearly with the environmental flow albeit at a faster speed (see, e.g., Fig. 7 of Chan and Gray, 1982). This means that in the frame of reference co-moving with the storm the environmental winds blow against the moving storm: area  $S$  in Fig. 8b is located in the two front quadrants of the moving storm (Fig. 17a). This moisture influx should produce more rain ahead of the cyclone center. This agrees with the findings of Lonfat et al. (2004) who established that in tropical cyclones there is more rainfall in the front two quadrants and less rainfall in the rear two quadrants of the moving storm.

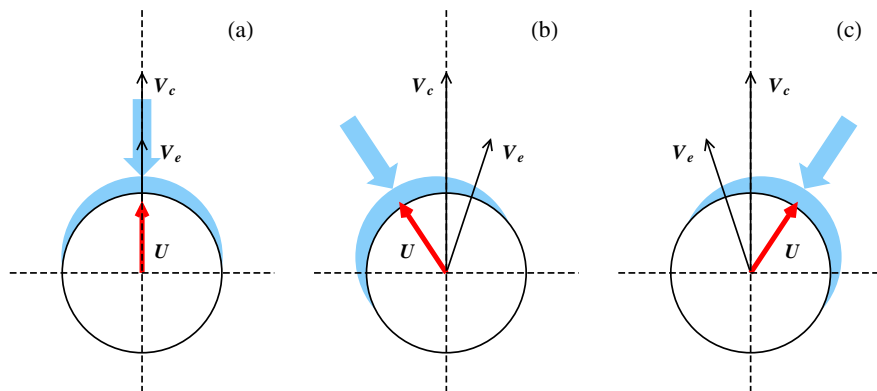


Figure 17: Predicted rainfall asymmetry (more rain is indicated by the blue area, cf. Fig. 8b) as dependent on propagation velocity  $\mathbf{U} = \mathbf{V}_c - \mathbf{V}_e$  in the inflow layer for different orientations of translation velocity  $\mathbf{V}_c$  of the cyclone relative to velocity  $\mathbf{V}_e$  of the environmental flow. Blue arrow indicates the dominant direction of moisture import into the cyclone associated with its movement.

If the hurricane moves to the right (left) of the low-level environmental flow, then

water vapor is predominantly imported into the front left (right) quadrant, producing more rain there (Fig. 17b,c). For eastward moving Atlantic cyclones Dong and Neumann (1986) indicated that while weakening storms tend to move to the left of the low-level environmental flow (Fig. 17b), intensifying storms as well as hurricanes tend to move to the right of it (Fig. 17c). This is consistent with the earlier findings of Miller (1958, Fig. 7) whereby in the lower 1-3 km radial velocity relative to the hurricane center is maximum in the front right quadrant. These differences may explain the variation in rainfall asymmetries between weak and intense storms (see Lonfat et al., 2004). The relationships between rainfall asymmetries and the vertical wind shear between the 850 hPa and 200 hPa investigated by Chen et al. (2006) may also reflect the dependence of rainfall on propagation velocity  $U$ , since the latter changes both its direction and magnitude with altitude (see, e.g., Dong and Neumann, 1986, their Fig. 2).

Asymmetries in the spatial distribution of ambient water vapor should be equally important to the water vapor budget. In our calculations we used the mean amount  $\sigma_0(r)$  of water vapor present in a hurricane-free environment. If, however, hurricanes predominantly move in the direction of a higher water vapor content this would mean that  $k$  in Eq. (7) is higher and the radius of self-sufficiency  $r_h$  is lower than we estimated. According to Fig. 8, what matters most is the water vapor content available to the cyclone in the direction of its propagation velocity.

The formulated view of the hurricane as an open system which maintains itself by continuously consuming atmospheric moisture as it moves explains the hurricane moisture budget and generally clarifies the nature of hurricanes as steady-state systems. In particular, Smith et al. (2014) indicated that the source of angular momentum for a steady-state hurricane remains unknown. That is, if we consider the air moving along path AB in Fig. 1, the angular momentum of this air is known to diminish with decreasing  $r$ . Since in the upper atmosphere angular momentum is approximately conserved as the air moves along path BCD, the question posed by Smith et al. (2014) was how, in a steady-state, the air gains angular momentum as it descends from D to F. Our view of the hurricane as an open system identifies such a source: it comes with external air. Having left the hurricane, the air does not return (Fig. 8a). In this framework, in the reference frame of the Earth the hurricane is not a steady-state circulation. It would vanish if its motion relative to the air discontinues or if it encounters a dry area.

While the fact that rainfall greatly exceeds evaporation in intense cyclones has been long recognized, it has also been maintained that, compared to evaporation, rainfall by itself does not play a significant role in cyclone formation (Malkus and Riehl, 1960; Emanuel, 1991; Gamache et al., 1993; Braun, 2006; Yang et al., 2011; Huang et al., 2014). This view stemmed from the observed relationship between the fall in surface pressure  $\Delta p$  (key for hurricane development) and water vapor increment in surface air  $\Delta \gamma$ . This relationship, usually expressed in terms of equivalent potential temperature, is conventionally interpreted as a cause-effect relationship: no evaporation, no pressure fall, no hurricane (Malkus and Riehl, 1960; Holland, 1997). We note, however, that this relation-

ship is similar to that between surface pressure and temperature gradients which we have debated elsewhere (Makarieva et al., 2015b). As we previously showed, such relationships are based on one key parameter – the isobaric height. Its magnitude is derived from observations and cannot prove cause-effect relationships among the variables in question. In other words, while it is commonly observed that the drop in surface pressure in intense hurricanes is accompanied by an increase in the moisture content  $\gamma$  of the surface air, this evaporation may as well be a result as well as a cause of the pressure change. Despite its long history, we find no evidence to indicate that the pressure gradients observed in intense cyclones could develop in the presence of intense evaporation without large-scale atmospheric moisture supplies (and related rainfall). But, in keeping with our interpretations, there is accumulating evidence to the contrary.

Intensity forecasts for tropical cyclones have been shown to be sensitive to the accurate representation of rainfall (Krishnamurti et al., 1993, 1998). Recent observations and modelling studies indicate a correlation between cyclone intensification and atmospheric moisture input (Fritz and Wang, 2014; Ermakov et al., 2014, 2015). Our theoretical framework indicates that hurricane intensity is directly proportional to rainfall (Eq. 16). Sabuwala et al. (2015) established this proportionality empirically. Here we have also shown that consideration of the atmospheric moisture supply and associated rainfall is key for constraining hurricane intensity. We thus call for a broader re-assessment of the role of the hurricane’s moisture dynamics in storm development and maintenance.

**Acknowledgments.** We thank B. Jaimes, L.K. Shay and E.W. Uhlhorn for providing us with the data of their Fig. 11 and M. Bell, M. Montgomery and K. Emanuel for providing us with the data of their Fig. 15. MERRA and TRMM data have been provided by the Global Modeling and Assimilation Office at NASA Goddard Space Flight Center through the NASA GES DISC online archive (<http://mirador.gsfc.nasa.gov>). This work is partially supported by Russian Scientific Foundation Grant 14-22-00281, the University of California Agricultural Experiment Station, the Australian Research Council project DP160102107 and the CNPq/CT-Hidro - GeoClima project Grant 404158/2013-7.

## References

- Anthes, R. A., 1974: The dynamics and energetics of mature tropical cyclones. *Rev. Geophys.*, **12**, 495–522, doi:10.1029/RG012i003p00495.
- Bell, M. M., M. T. Montgomery, and K. A. Emanuel, 2012: Air-sea enthalpy and momentum exchange at major hurricane wind speeds observed during CBLAST. *J. Atmos. Sci.*, **69**, 3197–3222, doi:10.1175/JAS-D-11-0276.1.
- Braun, S. A., 2006: High-resolution simulation of Hurricane Bonnie (1998). Part II: Water budget. *J. Atmos. Sci.*, **63**, 43–64, doi:10.1175/JAS3609.1.

- Carr III, L. E. and R. L. Elsberry, 1990: Observational evidence for predictions of tropical cyclone propagation relative to environmental steering. *J. Atmos. Sci.*, **47** (4), 542–546, doi:10.1175/1520-0469(1990)047<0542:OEFPOT>2.0.CO;2.
- Chan, J. C. L., 2005: The physics of tropical cyclone motion. *Annu. Rev. Fluid Mech.*, **37**, 99–128, doi:10.1146/annurev.fluid.37.061903.175702.
- Chan, J. C. L. and W. M. Gray, 1982: Tropical cyclone movement and surrounding flow relationships. *Mon. Wea. Rev.*, **110**, 1354–1374, doi:10.1175/1520-0493(1982)110<1354:TCMASF>2.0.CO;2.
- Chen, S. S., J. A. Knaff, and F. D. Marks Jr., 2006: Effects of vertical wind shear and storm motion on tropical cyclone rainfall asymmetries deduced from TRMM. *Mon. Wea. Rev.*, **134**, 3190–3208, doi:10.1175/MWR3245.1.
- DeMaria, M. and J. Kaplan, 1994: Sea surface temperature and the maximum intensity of atlantic tropical cyclones. *J. Climate*, **7**, 1324–1334, doi:10.1175/1520-0442(1994)007<1324:SSTATM>2.0.CO;2.
- Demuth, J. L., M. DeMaria, and J. A. Knaff, 2006: Improvement of advanced microwave sounding unit tropical cyclone intensity and size estimation algorithms. *J. Appl. Meteor. Climatol.*, **45**, 1573–1581, doi:10.1175/JAM2429.1.
- Dong, K. and C. J. Neumann, 1986: The relationship between tropical cyclone motion and environmental geostrophic flows. *Mon. Wea. Rev.*, **114**, 115–122, doi:10.1175/1520-0493(1986)114(0115:TRBTCM)2.0.CO;2.
- Emanuel, K. A., 1986: An air-sea interaction theory for tropical cyclones. Part I: Steady-state maintenance. *J. Atmos. Sci.*, **43**, 585–604, doi:10.1175/1520-0469(1986)043<0585:AASITF>2.0.CO;2.
- Emanuel, K. A., 1991: The theory of hurricanes. *Annu. Rev. Fluid Mech.*, **23**, 179–196.
- Emanuel, K. A., 1999: The power of a hurricane: An example of reckless driving on the information superhighway. *Weather*, **54**, 107–108, doi:10.1002/j.1477-8696.1999.tb06435.x.
- Ermakov, D. M., E. A. Sharkov, and A. P. Chernushich, 2014: The role of tropospheric advection of latent heat in the intensification of tropical cyclones. *Issledovanie Zemli iz Kosmosa, (Earth Research from Space)*, **4**, 3–15, doi:10.7868/S0205961414040046, (in Russian).
- Ermakov, D. M., E. A. Sharkov, and A. P. Chernushich, 2015: Satellite radiothermography of atmospheric mesoscale processes: case study of tropical cyclones. *Int. Arch. Photogramm. Remote Sens. Spatial Inf. Sci.*, **XL-7/W3**, 179–186, doi:10.5194/isprsarchives-XL-7-W3-179-2015.

- Frank, W. M., 1977: The structure and energetics of the tropical cyclone I. Storm structure. *Mon. Wea. Rev.*, **105**, 1119–1135, doi:10.1175/1520-0493(1977)105<1119: TSAEOT>2.0.CO;2.
- Franklin, J. L., S. E. Feuer, J. Kaplan, and S. D. Aberson, 1996: Tropical cyclone motion and surrounding flow relationships: Searching for beta gyres in Omega dropwind-sonde datasets. *Mon. Wea. Rev.*, **124**, 64–84, doi:10.1175/1520-0493(1996)124<0064: TCMASF>2.0.CO;2.
- Fritz, C. and Z. Wang, 2014: Water vapor budget in a developing tropical cyclone and its implication for tropical cyclone formation. *J. Atmos. Sci.*, **71**, 4321–4332, doi:10.1175/JAS-D-13-0378.1.
- Gamache, J. F., R. A. Houze Jr., and F. D. Marks Jr., 1993: Dual-aircraft investigation of the inner core of Hurricane Norbert. Part III: Water budget. *J. Atmos. Sci.*, **50**, 3221–3243, doi:10.1175/1520-0469(1993)050<3221:DAIOTI>2.0.CO;2.
- George, J. E. and W. M. Gray, 1976: Tropical cyclone motion and surrounding parameter relationships. *J. Appl. Meteor.*, **15**, 1252–1264, doi:10.1175/1520-0450(1976)015<1252: TCMASP>2.0.CO;2.
- Hawkins, H. F. and S. M. Imbembo, 1976: The structure of a small, intense hurricane – Inez 1966. *Mon. Wea. Rev.*, **104**, 418–442, doi:10.1175/1520-0493(1976)104<0418: TSOASI>2.0.CO;2.
- Hawkins, H. F. and D. T. Rubsam, 1968: Hurricane Hilda, 1964 II. Structure and budgets of the hurricane on October 1, 1964. *Mon. Wea. Rev.*, **96**, 617–636, doi: 10.1175/1520-0493(1968)096<0617:HH>2.0.CO;2.
- Holland, G., 2008: A revised hurricane pressure–wind model. *Mon. Wea. Rev.*, **136**, 3432–3445, doi:10.1175/2008MWR2395.1.
- Holland, G. J., 1984: Tropical cyclone motion: A comparison of theory and observation. *J. Atmos. Sci.*, **41**, 68–75, doi:10.1175/1520-0469(1984)041<0068:TCMACO>2.0.CO;2.
- Holland, G. J., 1997: The maximum potential intensity of tropical cyclones. *J. Atmos. Sci.*, **54**, 2519–2541, doi:10.1175/1520-0469(1997)054<2519:TMPIOT>2.0.CO;2.
- Huang, H.-L., M.-J. Yang, and C.-H. Sui, 2014: Water budget and precipitation efficiency of Typhoon Morakot (2009). *J. Atmos. Sci.*, **71**, 112–129, doi:10.1175/JAS-D-13-053.1.
- Huffman, G. J., 1997: Estimates of root-mean-square random error for finite samples of estimated precipitation. *J. Appl. Meteor.*, **36**, 1191–1201, doi:10.1175/1520-0450(1997) 036<1191:EORMSR>2.0.CO;2.



- Huffman, G. J., et al., 2007: The TRMM multisatellite precipitation analysis (TMPA): Quasi-global, multiyear, combined-sensor precipitation estimates at fine scales. *J. Hydrometeorol.*, **8**, 38–55, doi:10.1175/JHM560.1.
- Jaimes, B., L. K. Shay, and E. W. Uhlhorn, 2015: Enthalpy and momentum fluxes during Hurricane Earl relative to underlying ocean features. *Mon. Wea. Rev.*, **143**, 111–131, doi:10.1175/MWR-D-13-00277.1.
- Jiang, H., J. B. Halverson, J. Simpson, and E. J. Zipser, 2008: On the differences in storm rainfall from hurricanes Isidore and Lili. Part II: Water budget. *Wea. Forecasting*, **23**, 44–61, doi:10.1175/2007WAF2005120.1.
- Kieu, C., 2015: Revisiting dissipative heating in tropical cyclone maximum potential intensity. *Quart. J. Roy. Meteorol. Soc.*, **141**, 2497–2504, doi:10.1002/qj.2534.
- Krishnamurti, T. N., H. S. Bedi, and K. Ingles, 1993: Physical initialization using SSM/I rain rates. *Tellus A*, **45**, 247–269, doi:10.1034/j.1600-0870.1993.t01-3-00001.x.
- Krishnamurti, T. N., W. Han, and D. Oosterhof, 1998: Sensitivity of hurricane intensity forecasts to physical initialization. *Meteorol. Atmos. Phys.*, **65**, 171–181, doi:10.1007/BF01030786.
- Kurihara, Y., 1975: Budget analysis of a tropical cyclone simulated in an axisymmetric numerical model. *J. Atmos. Sci.*, **32**, 25–59, doi:10.1175/1520-0469(1975)032<0025:BAOATC>2.0.CO;2.
- Lonfat, M., F. D. Marks, Jr., and S. S. Chen, 2004: Precipitation distribution in tropical cyclones using the Tropical Rainfall Measuring Mission (TRMM) microwave imager: A global perspective. *Mon. Wea. Rev.*, **132**, 1645–1660, doi:10.1175/1520-0493(2004)132<1645:PDITCU>2.0.CO;2.
- Makarieva, A. M. and V. G. Gorshkov, 2009: Condensation-induced kinematics and dynamics of cyclones, hurricanes and tornadoes. *Phys. Lett. A*, **373**, 4201–4205, doi:10.1016/j.physleta.2009.09.023.
- Makarieva, A. M. and V. G. Gorshkov, 2011: Radial profiles of velocity and pressure for condensation-induced hurricanes. *Phys. Lett. A*, **375**, 1053–1058, doi:10.1016/j.physleta.2011.01.005.
- Makarieva, A. M., V. G. Gorshkov, B.-L. Li, and A. D. Nobre, 2010: A critique of some modern applications of the Carnot heat engine concept: the dissipative heat engine cannot exist. *Proc. R. Soc. A*, **466**, 1893–1902, doi:10.1098/rspa.2009.0581.



- Makarieva, A. M., V. G. Gorshkov, and A. V. Nefiodov, 2015a: Empirical evidence for the condensational theory of hurricanes. *Phys. Lett. A*, **379**, 2396–2398, doi:10.1016/j.physleta.2015.07.042.
- Makarieva, A. M., V. G. Gorshkov, A. V. Nefiodov, D. Sheil, A. D. Nobre, P. Bunyard, and B.-L. Li, 2013a: The key physical parameters governing frictional dissipation in a precipitating atmosphere. *J. Atmos. Sci.*, **70**, 2916–2929, doi:10.1175/JAS-D-12-0231.1.
- Makarieva, A. M., V. G. Gorshkov, A. V. Nefiodov, D. Sheil, A. D. Nobre, and B.-L. Li, 2015b: Comments on "The tropospheric land-sea warming contrast as the driver of tropical sea level pressure changes". *J. Climate*, **28**, 4293–4307, doi:10.1175/JCLI-D-14-00592.1.
- Makarieva, A. M., V. G. Gorshkov, D. Sheil, A. D. Nobre, and B.-L. Li, 2013b: Where do winds come from? A new theory on how water vapor condensation influences atmospheric pressure and dynamics. *Atmos. Chem. Phys.*, **13**, 1039–1056, doi:10.5194/acp-13-1039-2013.
- Malkus, J. S. and H. Riehl, 1960: On the dynamics and energy transformations in steady-state hurricanes. *Tellus*, **12**, 1–20, doi:10.1111/j.2153-3490.1960.tb01279.x.
- Miller, B. I., 1958: *The three-dimensional wind structure around a tropical cyclone*. Nat. Hurricane Res. Proj. Rep. 53, U.S. Dep. of Commer., Washington, D.C., 41 pp.
- Miller, B. I., 1962: *On the momentum and energy balance of hurricane Helene (1958)*. Nat. Hurricane Res. Proj. Rep. 53, U.S. Dep. of Commer., Washington, D.C., 19 pp.
- Montgomery, M. T., M. M. Bell, S. D. Aberson, and M. L. Black, 2006: Hurricane Isabel (2003): New insights into the physics of intense storms. Part I: Mean vortex structure and maximum intensity estimates. *Bull. Amer. Meteor. Soc.*, **87**, 1335–1347, doi:10.1175/BAMS-87-10-1335.
- Ozawa, H. and S. Shimokawa, 2015: Thermodynamics of a tropical cyclone: generation and dissipation of mechanical energy in a self-driven convection system. *Tellus A*, **67**, 24216, doi:10.3402/tellusa.v67.24216.
- Pauluis, O., 2011: Water vapor and mechanical work: A comparison of Carnot and steam cycles. *J. Atmos. Sci.*, **68**, 91–102, doi:10.1175/2010JAS3530.1.
- Rappaport, E. N., 2000: Loss of life in the United States associated with recent Atlantic tropical cyclones. *Bull. Amer. Meteor. Soc.*, **81**, 2065–2073, doi:10.1175/1520-0477(2000)081<2065:LOLITU>2.3.CO;2.
- Riehl, H. and J. Malkus, 1961: Some aspects of hurricane Daisy, 1958. *Tellus*, **13**, 181–213, doi:10.1111/j.2153-3490.1961.tb00077.x.

- Rienecker, M. M., et al., 2011: MERRA: NASA’s modern-era retrospective analysis for research and applications. *J. Climate*, **24**, 3624–3648, doi:10.1175/JCLI-D-11-00015.1.
- Rodgers, E. B., S. W. Chang, and H. F. Pierce, 1994: A satellite observational and numerical study of precipitation characteristics in Western North Atlantic tropical cyclones. *J. Appl. Meteor.*, **33**, 129–139, doi:10.1175/1520-0450(1994)033<0129:ASOANS>2.0.CO;2.
- Sabuwala, T., G. Gioia, and P. Chakraborty, 2015: Effect of rainpower on hurricane intensity. *Geophys. Res. Lett.*, **42**, 3024–3029, doi:10.1002/2015GL063785.
- Smith, R. K., M. T. Montgomery, and J. Persing, 2014: On steady-state tropical cyclones. *Quart. J. Roy. Meteorol. Soc.*, **140**, 2638–2649, doi:10.1002/qj.2329.
- Trenberth, K. E., A. Dai, R. M. Rasmussen, and D. B. Parsons, 2003: The changing character of precipitation. *Bull. Amer. Meteor. Soc.*, **84**, 1205–1217, doi:10.1175/BAMS-84-9-1205.
- Trenberth, K. E., C. A. Davis, and J. Fasullo, 2007: Water and energy budgets of hurricanes: Case studies of Ivan and Katrina. *J. Geophys. Res.: Atmospheres*, **112**, D23 106, doi:10.1029/2006JD008303.
- Yang, M.-J., S. A. Braun, and D.-S. Chen, 2011: Water budget of Typhoon Nari (2001). *Mon. Wea. Rev.*, **139**, 3809–3828, doi:10.1175/MWR-D-10-05090.1.
- Yasunaga, K., T. Miyajima, and M. Yamaguchi, 2016: Relationships between tropical cyclone motion and surrounding flow with reference to longest radius and maximum sustained wind. *SOLA*, **12**, 277–281, doi:10.2151/sola.2016-054.